Alpha-carboxy nucleoside phosphonates as universal nucleoside triphosphate mimics

Jan Balzarini[a,1], Kalyan Das[b,c], Jean A. Bernatchez[d], Sergio E. Martinez[b,c], Marianne Ngure[e,f], Sarah Keane[g], Alan Ford[g], Nuala Maguire[g], Niki Mullins[g], Jubi John[h], Youngju Kim[h], Wim Dehaen[h], Johan Vande Voorde[a], Sandra Liekens[a], Lieve Naesens[a], Matthias Götte[d,e,f,i,2], Anita R. Maguire[g], and Eddy Arnold[b,c]

[a]Rega Institute for Medical Research and [h]Department of Chemistry, KU Leuven, B-3000 Leuven, Belgium; [b]Center for Advanced Biotechnology and Medicine and [c]Department of Chemistry and Chemical Biology, Rutgers University, Piscataway, NJ 08854-8020; [d]Department of Biochemistry, McGill University, Montreal, QC H3G 1Y6, Canada; [e]Department of Microbiology and Immunology, McGill University, Montreal, QC H3A 2B4, Canada; [f]Department of Medical Microbiology and Immunology, University of Alberta, Edmonton, AB T6G 2E1, Canada; [g]Department of Chemistry and School of Pharmacy, Analytical and Biological Chemistry Research Facility, Synthesis and Solid State Pharmaceutical Centre, University College Cork, Cork, Ireland; and [i]Department of Medicine, Division of Experimental Medicine, McGill University, Montreal, QC H3A 1A3, Canada

Edited by John M. Coffin, Tufts University School of Medicine, Boston, MA, and approved February 6, 2015 (received for review October 22, 2014)

Polymerases have a structurally highly conserved negatively charged amino acid motif that is strictly required for Mg^{2+} cation-dependent catalytic incorporation of (d)NTP nucleotides into nucleic acids. Based on these characteristics, a nucleoside monophosphonate scaffold, α-carboxy nucleoside phosphonate (α-CNP), was designed that is recognized by a variety of polymerases. Kinetic, biochemical, and crystallographic studies with HIV-1 reverse transcriptase revealed that α-CNPs mimic the dNTP binding through a carboxylate oxygen, two phosphonate oxygens, and base-pairing with the template. In particular, the carboxyl oxygen of the α-CNP acts as the potential equivalent of the α-phosphate oxygen of dNTPs and two oxygens of the phosphonate group of the α-CNP chelate Mg^{2+}, mimicking the chelation by the β- and γ-phosphate oxygens of dNTPs. α-CNPs (*i*) do not require metabolic activation (phosphorylation), (*ii*) bind directly to the substrate-binding site, (*iii*) chelate one of the two active site Mg^{2+} ions, and (*iv*) reversibly inhibit the polymerase catalytic activity without being incorporated into nucleic acids. In addition, α-CNPs were also found to selectively interact with regulatory (i.e., allosteric) Mg^{2+}-dNTP-binding sites of nucleos(t)ide-metabolizing enzymes susceptible to metabolic regulation. α-CNPs represent an entirely novel and broad technological platform for the development of specific substrate active- or regulatory-site inhibitors with therapeutic potential.

(deoxy)nucleoside triphosphate mimic | HIV reverse transcriptase | herpes virus DNA polymerase | allosteric inhibition | alpha-carboxy nucleoside phosphonate

A wide variety of proteins and enzymes specifically recognize (2′-deoxy)nucleoside 5′-triphosphates [(d)NTPs]. Nucleic acid polymerases are among the best known examples, and HIV-encoded reverse transcriptase (RT) is perhaps the best studied and established enzyme in this regard.

The polymerization of nucleotides by *Escherichia coli* DNA polymerase I represents a general model for catalytic action of nucleic acid polymerases (*SI Appendix*, Fig. S1) (1, 2). According to this model, there is a universal role for the Mg^{2+} cation to interact with three phosphate oxygens of dNTP. The highly conserved consensus motifs in every polymerase active site consist of either aspartate or glutamate residues that chelate Mg^{2+} through three additional coordination bonds during polymerization (2, 3). The crucial role of the metal cofactor and structurally conserved active site architecture in polymerases has also been demonstrated by validating Mg^{2+} as a target for the design of antiviral drugs, not only against HIV RT but also, among others, against HIV integrase, HIV ribonuclease H (RNase H), and influenza-encoded endonuclease (4, 5). Hence, it should be feasible to design a universal but simplified (d)NTP mimic that binds efficiently to a wide variety of DNA/RNA polymerases.

It was hypothesized that a universal nucleoside triphosphate mimic should contain three major indispensable entities: (*i*) a nucleobase part (i.e., to achieve optimal Watson–Crick base-pairing with the template overhang), (*ii*) a replacement of the triphosphate moiety that should enable efficient Mg^{2+}-directed coordination, and (*iii*) a variable linker between the nucleobase and the modified triphosphate to mimic the pentose entity present in natural (d)NTPs. For the triphosphate part, we chose an α-carboxy phosphonate entity that is chemically stable in physiological media and cannot be released from the triphosphate mimic by cellular (hydrolytic) enzymes. It was assumed that the carboxylate in the phosphonate moiety might help to coordinate Mg^{2+}. The phosphonate moiety, such as in the clinically used tenofovir (6), was chosen (instead of a phosphoester) to provide additional metal chelation affinity and to confer stability by preventing enzymatic hydrolysis. Given the fact that (2-deoxy)ribose, the most logical linker entity between nucleobase and phosphonate, could not be synthetically incorporated due to the intrinsic lability of the ether oxygen bridge that links the pentose to the phosphonate, a cyclopentyl ring was initially introduced as the

Significance

The polymerization of nucleotides by DNA polymerases occurs through a common mechanism based on similar highly conserved amino acid motifs and the universal role of the coordination of Mg^{2+} by three dNTP phosphate oxygens. Based on these universal principles, we aimed at designing a dNTP mimic that could interact with a broad variety of DNA polymerases and should consist of three major indispensable entities: a nucleobase for Watson–Crick base-pairing, an enzymatically and chemically stable triphosphate replacement that can efficiently coordinate the Mg^{2+} cation, and a variable linker moiety between the nucleobase and the modified phosphate. The resulting α-carboxy nucleoside phosphonates (α-CNPs) were structurally, kinetically, and biochemically investigated, and the novel dNTP mimics were successfully validated in several DNA polymerase models.

Author contributions: J.B., K.D., J.A.B., S.E.M., S.K., A.F., N. Maguire, N. Mullins, J.J., Y.K., W.D., J.V.V., S.L., L.N., M.G., A.R.M., and E.A. designed research; K.D., J.A.B., S.E.M., M.N., S.K., A.F., N. Maguire, N. Mullins, J.J., Y.K., J.V.V., and L.N. performed research; J. Balzarini, K.D., J.A.B., S.E.M., S.K., A.F., N. Mullins, J.J., Y.K., W.D., J.V.V., S.L., L.N., M.G., A.R.M., and E.A. analyzed data; and J.B., K.D., M.G., A.R.M., and E.A. wrote the paper.

Conflict of interest statement: J.B., W.D., A.R.M., S.K., A.F., N. Maguire, and N. Mullins are coinventors of a patent filing on the α-CNPs.

This article is a PNAS Direct Submission.

Data deposition: The coordinates and structure factors for the HIV-1 RT/dsDNA/T-α-CNP complex have been deposited in the Protein Data Bank, www.pdb.org (PDB ID code 4R5P).

[1]To whom correspondence should be addressed. Email: jan.balzarini@rega.kuleuven.be.

[2]Present address: Department of Medical Microbiology and Immunology, University of Alberta, Edmonton, AB T6G 2E1, Canada.

This article contains supporting information online at www.pnas.org/lookup/suppl/doi:10.1073/pnas.1420233112/-/DCSupplemental.

linker moiety, as has been done before for the HIV-1 nucleoside RT inhibitor (NRTI) carbovir (7).

To investigate and validate the design of a universal (d)NTP mimic, we chose the well-characterized HIV-1 RT as a preferred model system, as a variety of kinetic, biochemical, and structural tools are available and well-established to study this enzyme.

Results

Kinetic Studies. The thymine (T)-, uracil (U)-, cytosine (C)-, and adenine (A)-α-CNP (α-carboxy nucleoside phosphonate) derivatives were synthesized and examined for their interaction with HIV-1 RT. The α-CNPs were initially investigated not only as their racemic dextrorotatory/levorotatory (D/L) (1:1) mixtures but also as pure D- and L-enantiomers in the presence of three different homopolymeric template/primers (i.e., poly rA.dT, poly rI.dC, and poly rU.dA) and their corresponding [CH_3-^{3}H]dTTP, [5-^{3}H]dCTP, and [2,8-^{3}H]dATP substrates. Each of the α-CNP enantiomers represents a pair of diastereomers at the alpha-carboxy stereocenter. The D-enantiomers showed poor, if any, inhibitory activity against HIV-1 RT, whereas the D/L-racemic mixtures (8) and the pure L-enantiomers markedly inhibited HIV-1 RT at concentrations (IC_{50}, 0.19–4.3 μM) that were on the same order of magnitude as the respective reference compounds AZT-triphosphate (TP), ddCTP, and ddATP (IC_{50}, 0.11–14 μM) (Table 1 and *SI Appendix*, Table S1). Pronounced enzyme inhibition was found only when the α-CNPs contained the same natural nucleobase as the competing radiolabeled dNTP substrate. The template/primer-specific inhibition of HIV-1 RT by α-CNPs strongly suggests that α-CNPs compete with the natural dNTP substrate for binding to the enzyme. This conclusion was further substantiated in more detailed kinetic experiments using different homopolymeric template/primers and their corresponding dNTP substrates, as evident from the substrate versus velocity plots in *SI Appendix*, Fig. S2*A* and the kinetic calculations using the mixed model inhibition of GraphPad (*SI Appendix*, Table S2). These plots also revealed mixed-type (close-to-uncompetitive) inhibition of RT against the template/primer by T-α-CNP (*SI Appendix*, Fig. S2*B*), which indicates that binding of template/primer to HIV-1 RT is required before efficient binding of the α-CNP to the enzyme. Although structurally distinct, the α-CNP inhibition kinetics (*SI Appendix*, Fig. S2 *A* and *B*) resembled not only those of the well-known DNA chain-terminating NRTI AZT-TP (*SI Appendix*, Fig. S2 *C* and *D*) (11) but also those of the nucleotide-competing RT inhibitor (NcRTI) INDOPY-1 (*SI Appendix*, Fig. S2 *E* and *F*). INDOPY-1 is the prototype compound of a well-defined class of nonnucleoside indolopyridinones that interact—like NRTIs—with the substrate active site of HIV RT in a competitive manner with the natural dNTP substrates (12).

L-enantiomeric α-CNPs were also found to be inhibitory against a broad variety of other lentiviral RTs (Table 1), mostly, like nucleo(s)(t)ide RT inhibitors (N(t)RTIs), within the same order of magnitude. Given the highly conserved structural motifs (i.e., Asp/Glu residues) and functional coordination properties of Mg^{2+} in the polymerase active sites, we hypothesized that α-CNPs that function as (d)NTP mimics should also inhibit other polymerases. The interactions of the T-, C-, and A-α-CNP derivatives with several herpetic DNA polymerases were therefore investigated. As evident from Table 1, α-CNPs indeed interact with the herpetic DNA polymerases and also, but less strongly, with the cellular DNA polymerases α and β. The inhibitory activities of the triphosphate of the retroviral AZT (zidovudine), the herpetic (*E*)-5-(2-bromovinyl)-2′-deoxyuridine (BVDU, brivudine), and the pyrophosphate analog phosphonoformic acid (PFA, foscarnet) inhibitors have been included as controls (Table 1). AZT-TP proved 4- to 50-fold more inhibitory to the lentiviral RTs, BVDU-TP was 10- to 100-fold more inhibitory to the herpetic DNA polymerases, whereas PFA was equally inhibitory against HIV-1 RT and FIV RT, 30-fold more inhibitory against HIV-2 RT and SIV RT, four- to eightfold more inhibitory to HCMV and HSV-1 DNA polymerase, and 200-fold more inhibitory to VZV DNA polymerase than T-α-CNP. Instead, the reference compounds BVDU-TP and PFA were markedly more inhibitory against the cellular DNA polymerase α than the α-CNPs (Table 1).

Although the affinity of the α-CNPs was clearly superior for HIV-1 RT, followed by herpetic DNA polymerases, and lowest for the cellular DNA polymerases, it should be taken into account that the pentose mimicking (cyclopentyl) part of the α-CNP is more suited to inhibit RTs (mimicking a 2′,3′-dideoxyribose) and least appropriate for inhibiting the cellular DNA polymerases α and β, which prefer an intact 2-deoxyribose. Taking this in mind, an acyclic α-CNP has been designed (*SI Appendix*, Fig. S3) containing an aliphatic butenyl bridge. Such an aliphatic (acyclic) moiety has previously been shown to generate compounds with antiherpetic activity (13). This modified α-CNP indeed demonstrated a pronounced inhibition of all three herpetic DNA polymerases, and its inhibitory activity was by far superior (selective) for these viral enzymes compared with HIV RT and DNA polymerase

Table 1. Inhibitory activity of the L-enantiomeric α-CNPs against various lentiviral RTs and other DNA polymerases*

	IC_{50}† DNA polymerase, μM					
Enzyme source	T-α-CNP	C-α-CNP	A-α-CNP	BVDU-TP	AZT-TP	PFA
HIV-1 RT	0.41 ± 0.08	4.3 ± 0.3	0.19 ± 0.11	0.89 ± 0.04	0.11 ± 0.05	0.34 ± 0.01
HIV-2 RT	4.4 ± 1.9	22 ± 4.9	0.43 ± 0.05	2.6 ± 1.2	0.08 ± 0.03	0.16 ± 0.09
SIV RT	1.3 ± 0.6	20 ± 11	0.43 ± 0.00	4.6 ± 2.1	0.09 ± 0.01	0.05 ± 0.01
FIV RT	0.49 ± 0.05	11 ± 8	2.1 ± 0.8	2.6 ± 0.6	0.07 ± 0.02	0.59 ± 0.07
Visna RT	4.1 ± 1.1	46 ± 6	0.16 ± 0.06	—	0.09 ± 0.01	—
HCMV DNA polymerase	38 ± 11	17 ± 11	23 ± 6.7	3.6 ± 0.7	>100	9.8 ± 5.8
HSV-1 DNA polymerase	26 ± 20	19 ± 2	3.5 ± 1.1	0.75‡	—	3§
VZV DNA polymerase	38 ± 16	—	—	0.49 ± 0.09	5.7 ± 3.2	0.18 ± 0.01
DNA polymerase α	229 ± 27	269 ± 89	171 ± 21	21 ± 10	>100	7.7 ± 6.5
DNA polymerase β	>200	≥200	>200	26 ± 4	≥200	>200

*Each α-CNP represents a pair of diastereomers at the alpha-carboxy stereocenter.
†Fifty percent inhibitory concentration required to inhibit polymerase activity by 50%. Shown are mean ± SD values of at least 2–4 independent experiments.
‡IC_{50} value was taken from ref. 9. The IC_{50}s of BVDU-TP for cellular DNA pol α and β were 9.2 and 47 μM, respectively, using similar assay conditions.
§IC_{50} value was taken from ref. 10.

α (Table 2). Thus, marked selectivity and preferential interaction with well-defined polymerases can be obtained by fine-tuning the α-CNP scaffold to the particular target (polymerase) enzymes.

Biochemical Studies. To provide more detailed mechanistic insight, inhibition of DNA synthesis was studied in gel-based assays. Dose–response experiments were performed with heteropolymeric DNA/DNA substrates that offer multiple binding sites for inhibitor and natural substrates (Fig. 1*A* and *SI Appendix*, Fig. S4). T-, C-, or A-containing α-CNPs (pure L-enantiomers) show inhibition patterns that reflect the different nature of the nucleobase. Inhibition of DNA synthesis is always observed at a single site before the predicted location at which the competitive inhibitor interacts with its natural template nucleobase counterpart (Fig. 1*A*). This also demonstrates that α-CNPs are not incorporated into the growing DNA chain, which would have changed the primer migration. Time-course experiments at a fixed concentration of α-CNPs revealed that inhibition is reversible (*SI Appendix*, Fig. S4). In the presence of the respective T-, C-, or A-containing α-CNPs, the formation of the full-length product was significantly delayed, in favor of multiple abortive products. The short reaction products disappeared as a function of time, which is indicative of enzyme pausing and reversible inhibition. Hence, the mechanism of α-CNP inhibition does not involve DNA chain termination as demonstrated for N(t)RTIs (7, 11). Rather, the RT inhibition by α-CNPs is reminiscent of the mechanism of action described for INDOPY-1 (12) and involves reversible competition at or in close proximity to the dNTP-binding site.

Next, it was investigated if α-CNPs are capable of forming stable ternary complexes, as demonstrated for nucleotides and INDOPY-1. Complex formation was monitored with increasing concentrations of C-α-CNP against four different template/primer combinations that contained either T, A, G, or C in the template overhang at the nucleotide-binding site (Fig. 1*B*). Stable, heparin-resistant ternary complexes were only seen with a templating guanine base, which is strongly indicative for specific Watson–Crick base-pairing. These findings contrast with the NcRTI INDOPY-1, which was able to form a stable ternary complex irrespective of the nature of the templating nucleotide base (*SI Appendix*, Fig. S5).

Finally, the influence of the inhibitor on the precise position of HIV-1 RT on its template/primer was studied through Fe^{2+}-mediated, high-resolution footprinting. Upon binding of Fe^{2+} ions to the RNase H domain of HIV-1 RT, the template is cut in a site-specific manner that enables the distinction between pre- and posttranslocational conformations of the RT–template/primer complex (14). The enzyme shuttles between the two positions and accommodates either the 3′ end of the primer (pretranslocation) or the nucleotide substrate (posttranslocation) at the active site. Increasing concentrations of C-α-CNP shift this dynamic equilibrium toward posttranslocation (*SI Appendix*, Fig. S6). Thus, α-CNPs, like natural dNTP substrates and like INDOPY-1 (12), bind to, and trap, the posttranslocational RT conformation.

Structural Studies. The crystal structure of the HIV-1 RT/dsDNA/T-α-CNP ternary complex was determined at 2.9 Å resolution (Fig. 2*A* and *SI Appendix*, Fig. S7 and Table S3). In agreement with the kinetic data, the structure revealed the binding of T-α-CNP at the dNTP-binding site (*N* site) of an RT/dsDNA posttranslocational complex. Mimicking a dNTP, (*i*) the thymine part of T-α-CNP is base-paired with the template adenine base overhang; (*ii*) the cyclopentyl ring interacts with Y115, Q151, and M184 from three sides in a manner analogous to the interactions of the 2′-deoxyribose ring of a dNTP; and (*iii*) the carboxymethylphosphonate part chelates a Mg^{2+} ion (metal B) at the polymerase active site. In general, binding of T-α-CNP is analogous to a dNTP and distinct from a pyrophosphate (or foscarnet), which binds the pretranslocated RT/nucleic acid complex at a location that can be occupied by the pyrophosphate (PPi) leaving group (15).

The most striking feature is the unusual and unexpected mode of chelation of the α-carboxy-phosphonate at the polymerase active site. Two oxygens of the phosphonate group of α-CNP chelate metal B, replacing the chelation by β- and γ-phosphate oxygens of a dNTP. A carboxyl oxygen of α-CNP is the positional equivalent of the α-phosphate oxygen of dNTP that chelates both metals A and B. The positions and orientations of the catalytic residues (D110, D185, and D186) in the T-α-CNP complex superimpose well with those in RT/nucleic acid/dNTP (or analog) ternary complexes (*SI Appendix*, Fig. S7). However, like in most of the crystal structures of RT/dsDNA/dNTP (or analog) complexes (16), electron density for metal A is not observed. Thereby, the α-CNP in the current structure maintains a complete octahedral coordination environment for the catalytic metal ion B and satisfies the geometrical and chemical requirements to involve the metal ion A (Fig. 2*B*). Unlike a triphosphate moiety, the chelated α-carboxy-phosphonate group does not contain a phosphodiester bond for hydrolysis by RT, and thereby, α-CNP forms a nonproductive ternary complex state with RT, leading to inhibition. This fundamental and indispensable role of the Mg^{2+}-coordinating capacity of the three oxygens in the α-CNP is further confirmed by the demonstration that modifying one of these three oxygen atoms in the α-CNP with a methyl group such as in the mono- and trimethylated T-α-CNP (*SI Appendix*, Figs. S3 and S7) completely obliterated the interaction of the compounds with HIV RT (IC_{50} > 100 μM). Thus, α-CNPs are entirely novel, efficient, and simplified mimics of the natural dNTP substrates that inhibit HIV-1 RT as competitive inhibitors.

Sensitivity Against HIV-1 RT with Known Resistance-Conferring Mutations. Like NRTIs, α-CNPs are sensitive to RT mutations adjacent to the pentose/cyclopentyl ring. The mutation M184V confers 1.7- to 16-fold resistance to α-CNPs depending on the nature of the nucleobase in the α-CNP (*SI Appendix*, Table S4). The M184V mutation has also been reported to confer resistance of HIV-1 RT to INDOPY-1 (17), and earlier also to the L-nucleoside inhibitors lamivudine (3TC) and emtricitabine (FTC) (18). This resistance was shown to be due to steric hindrance of the L-sugar ring by the 184-valine side chain (19). The crystal structure suggests a similar mechanism of resistance for α-CNPs by the M184V mutation in HIV-1 RT. Another mutation,

Table 2. Inhibitory activity of acyclic T-butenyl-α-CNP and T-cyclopentyl-α-CNP against various DNA polymerases

	IC_{50}* DNA polymerase, μM				
	HIV-1 RT	HCMV DNA pol	HSV-1 DNA pol	VZV DNA pol	DNA pol α
Acyclic T-butenyl-α-CNP	235 ± 16	2.1 ± 0.6	3.7 ± 1.7	2.2 ± 0.1	14 ± 7
T-α-CNP	0.41 ± 0.10	38 ± 11	26 ± 20	38 ± 16	229 ± 27

*Fifty percent inhibitory concentration required to inhibit enzyme activity by 50%. Mean ± SD values of at least 2–3 independent experiments are shown.

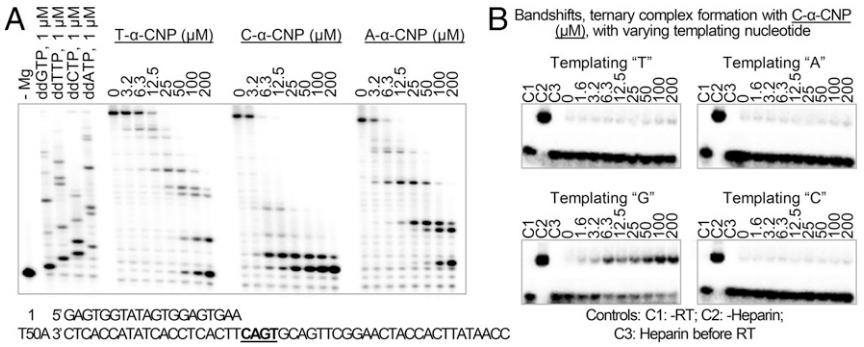

Fig. 1. Inhibition of HIV-1 RT-catalyzed DNA synthesis by α-CNPs. (*A*) Inhibition of DNA synthesis monitored in dose–response experiments in the presence of a fixed dNTP concentration, T50A DNA template/5′-radiolabeled P1 DNA primer, and increasing concentrations of T-, C-, and A-α-CNP, respectively (right block). Specific sites of inhibition by each of the three compounds are located a single residue before the inhibitor- and dNTP-binding sites. The left block shows control reactions with the obligate DNA chain-terminating ddNTPs. (*B*) Ternary RT template/primer inhibitor complex formation. Specific α-CNP binding to HIV-1 RT was analyzed with four different template/primer combinations that contain either a T-, A-, G-, or C-nucleotide, downstream of the 3′-primer end. Complex formation with HIV-1 RT was monitored with increasing C-α-CNP concentrations.

Y115F, demonstrated diminished inhibitory activity of the NcRTI INDOPY-1 against HIV-1 RT (17), however the mutation had no noticeable impact on the inhibitory activity of the C- and A-α-CNPs (*SI Appendix*, Table S4). The decreased inhibitory activity of INDOPY-1 against mutant Y115F HIV-1 RT has been earlier ascribed to the increased binding efficiency of the natural dNTP (but not INDOPY-1) to the mutant enzyme (16). These findings strongly suggest that the affinity of RT for α-CNPs is similarly increased in the mutant RT enzyme as observed for the dNTPs. The sensitivity data obtained for the Y115F and M184V RT mutants confirm again that α-CNPs act as novel dNTP mimics in the substrate active site of HIV-1 RT that is lined by both Y115 and M184.

Interference of α-CNPs with dNTP-Driven Enzyme Regulation. For a wide variety of enzymes, the activity is controlled by their reaction products or metabolic end-products through feedback or allosteric regulation. Well-known examples in nucleotide metabolism are inhibition of cytosolic thymidine (dThd) kinase 1 (TK-1) and mitochondrial TK-2 by Mg^{2+}-dTTP; TK-2 and dCyd kinase inhibition by Mg^{2+}-dCTP; dCMP deaminase (dCMPD) stimulation by Mg^{2+}-dCTP; ribonucleotide reductase regulation by Mg^{2+}-bound dNTP and ATP; and allosteric activation of dNTP hydrolase by (d)GTP (20–24). Therefore, the potential of α-CNPs to act as dNTP mimics in such enzymatic regulation processes was also investigated.

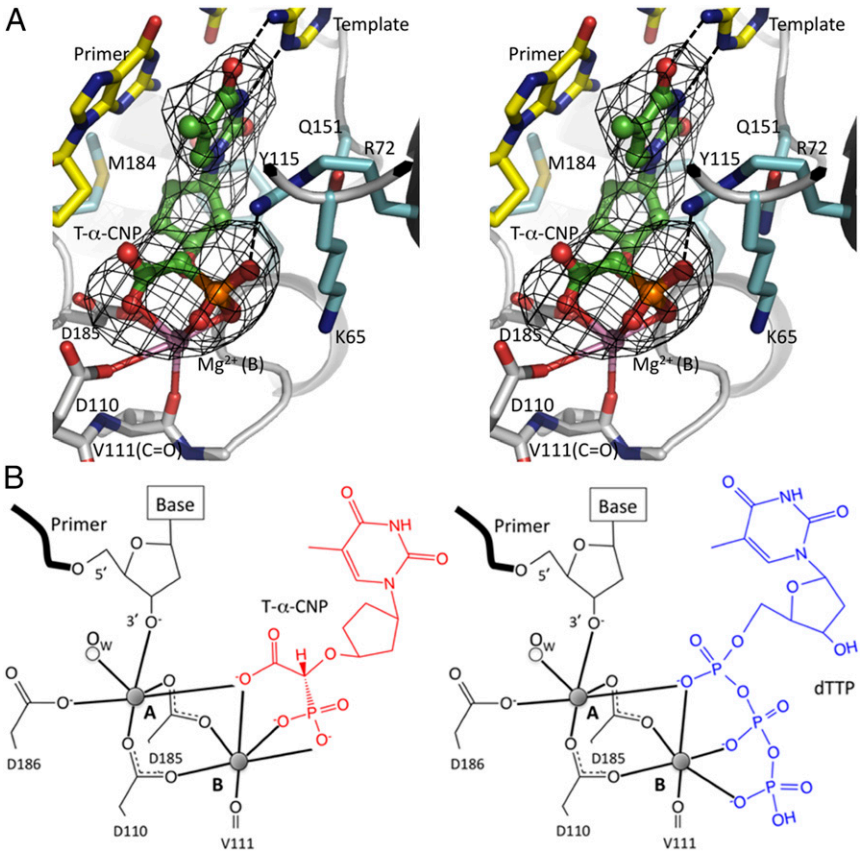

Fig. 2. Molecular interactions of T-α-CNP with HIV-1 RT. (*A*) A stereoview showing the binding of T-α-CNP at the polymerase active site in the crystal structure of HIV-1 RT in complex with a template/primer and T-α-CNP. The template overhang was designed to have an adenine base overhang for base-pairing with T-α-CNP. The 2.9 Å difference electron density (|Fo| – |Fc|) map contoured at 3 σ reveals the binding of T-α-CNP. Interacting residues of RT surrounding T-α-CNP are in cyan. The metal ion B has distorted octahedral coordination involving three oxygens of T-α-CNP, side chains of catalytic aspartates D110 and D185, and main chain C = O of V111. (*B*) A schematic comparison of the structural interactions of T-α-CNP (*Left*) and the natural dTTP (*Right*) with HIV-1 RT and the template/primer. The interactions shown are, in part, derived from the crystal structure coordinates as displayed in *A*. Because metal ion A was not observed in the crystal structure, the presumed interaction of metal ion A with D186, the 3′-OH end of the primer, and the oxygens of D110, D185, and the α-COOH of T-α-CNP is shown in the *Left* panel, by analogy with what has been demonstrated before for dNTPs (i.e., dTTP). The octahedral coordination of Mg^{2+} (metal ion B) reveals the participation of the carboxylate oxygen mimicking the interaction of the α-phosphate with Mg^{2+} and the participation of two phosphonate oxygens mimicking the interaction of the β- and γ-phosphates with Mg^{2+}. A structural superposition in *SI Appendix*, Fig. S7 compares the binding of T-α-CNP with a dNTP.

Interestingly, T-α-CNP, but not C- and A-α-CNPs, dose-dependently inhibited TK-2–catalyzed dThd phosphorylation (Fig. 3). The natural metabolic end-product inhibitor Mg^{2+}-dTTP suppressed the enzyme at a ∼20-fold lower concentration (IC_{50}, ∼2.5 μM). The herpesvirus TKs were less sensitive to the inhibitory action of dTTP and α-CNPs. In contrast with TK-2, TK-1 was not inhibited by T-α-CNP (IC_{50}, >200 μM), although Mg^{2+}-dTTP showed a pronounced feedback inhibition of the enzyme (IC_{50}, 1.5 μM) (Fig. 3 and *SI Appendix*, Fig. S8). T-α-CNP behaved as a noncompetitive inhibitor of TK-2 in the presence of dThd and thus might interact at a regulatory binding site (*SI Appendix*, Fig. S8 and Table S5) (25). Our kinetic findings are indeed strongly suggestive for specific recognition of T-α-CNP by TK-2. The complete lack of inhibitory activity of T-α-CNP against TK-1 may be related to the fact that TK-1 belongs to the type I class of TKs and structurally differs from type II class TK-2 and herpetic TKs (26). It has been demonstrated that the nucleobase of the natural allosteric TK inhibitor dTTP is hydrogen-bonded to main-chain atoms in TK-1, in contrast to other nucleoside kinases where specific interaction occurs with amino acid side chains (26).

The C-α-CNP derivative was found to interact with the stimulatory allosteric Mg^{2+}-dCTP binding site on dCMPD. In the absence of dCTP, dCMPD activity could be hardly observed. Instead, in the presence of 250 μM dCTP, a pronounced deamination of dCMP was found that linearly proceeded up to a dCMP concentration of 100 μM (*SI Appendix*, Fig. S8). Unlike dCTP, C-α-CNP did not stimulate dCMPD activity per se but instead markedly inhibited the Mg^{2+}-dCTP–driven enzyme activity (*SI Appendix*, Fig. S8). It was also ascertained that C-α-CNP did not act as a substrate for dCMPD. The dose-dependent inhibition profiles of C-α-CNP against dCMPD in the presence of a fixed dCTP (250 μM) concentration were remarkably similar at varying dCMP concentrations. Thus, our findings indicate that C-α-CNP selectively interacts with the allosteric stimulatory (Mg^{2+}-dCTP) binding site of dCMPD by antagonizing the dCTP stimulatory effect without being able to stimulate enzyme activity per se.

The interference of α-CNPs with allosteric inhibitory or stimulatory activities of (d)NTP-binding proteins may have therapeutic potential, as it has been previously demonstrated that dCTP not only stimulates the conversion of dCMP into dUMP (21) but also the conversion of the anticancer cytosar (araCMP) and gemcitabine (dFdCMP) metabolites to their inactive uridylate derivatives (27, 28). α-CNP may prevent such inactivation by its antagonistic potential.

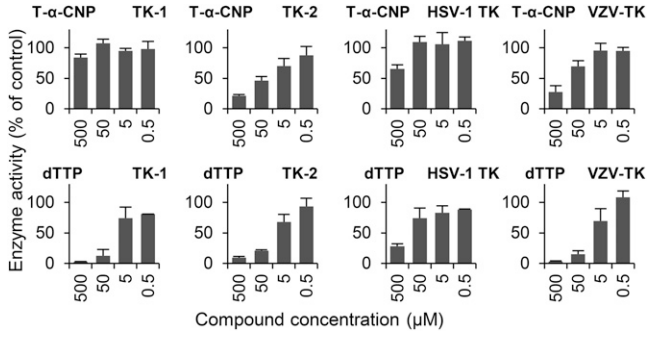

Fig. 3. Allosteric inhibition of TK by T-α-CNP and dTTP. Exposure of the L-enantiomeric T-, C-, and A-α-CNPs to cytosolic TK-1, mitochondrial TK-2, HSV-1 TK, and varicella-zoster virus TK at varying α-CNP concentrations (*Upper* panels). The natural feedback regulatory inhibitor dTTP was included as a positive control (*Lower* panels). Whereas Mg^{2+}-dTTP potently inhibited TK-1, TK-2, and VZV TK, T-α-CNP markedly suppressed TK-2 and VZV TK activity but not TK-1.

Studies on Intact Cells, Crude Cell Extracts, and Purified Enzymes. The T-α-CNP, C-α-CNP, and A-α-CNP derivatives were exposed to exponentially growing human $CD4^+$ T lymphocyte CEM and cervix carcinoma HeLa cell cultures but also confluent (monolayer) human lung fibroblast HEL and HeLa cell cultures for 3–4 d. None of the compounds were cytostatic or cytotoxic at 200 μM. They were also evaluated for potential anti–HIV-1 and anti–HIV-2 activity in human $CD4^+$ T-lymphocyte CEM cell cultures and for anti–HSV-1 and anti–HSV-2 activity in human embryonic lung HEL fibroblasts, but found inactive at the highest concentration tested (200 μM).

To reveal whether cellular enzymes may further metabolize (i.e., phosphorylate) the α-CNPs, CEM cell extracts but also purified recombinant UMP/CMP kinase and NDP kinase were administered to 100 μM T-α-CNP, U-α-CNP, C-α-CNP, or A-α-CNP in the presence of ATP and incubated for up to 6 h at 37 °C. They were not able to convert the compounds to a phosphorylated derivative, as inspected by HPLC analysis. Instead, 100 μM CMP or UMP was fully converted to cytidine diphosphate (CDP) or UDP by UMP/CMP kinase, and 100 μM thymidine diphosphate (dTDP), CDP, or adenosine diphosphate (ADP) was efficiently converted to their triphosphate derivatives by NDP kinase within 1 h of incubation.

Discussion

Kinetic, biochemical, and structural studies revealed that α-CNPs represent a novel synthetic scaffold and technological platform for designing specific tailor-made polymerase inhibitors that make use of both the highly conserved architecture and amino acid motifs in nucleic acid polymerases and the central role that hexa-coordinated Mg^{2+} plays in the catalytic activity of the polymerases. The α-CNPs function as efficient (d)NTP mimics in which one of the carboxylate oxygens and two phosphonate oxygens are of crucial importance in coordinating Mg^{2+} ions. The α-CNPs are the first (d)NTP mimics that structurally consist of a simple nucleoside monophosphonate scaffold not requiring further metabolic conversion (phosphorylation) for interaction with the target enzymes. Their mechanism of action, structural interaction with HIV-1 RT, and kinetic/biochemical properties are unique and differ from all known polymerase inhibitor classes of compounds (*SI Appendix*, Table S6).

The demonstration that α-CNPs inhibit different polymerases and enzymes that contain regulatory dNTP-binding sites is unique from a fundamental viewpoint and may also have important translational and chemotherapeutic implications. The α-CNPs can be used to study allosteric (dNTP) site binding effects leading to selective antagonistic inhibition or activation of enzyme activity. It has indeed been shown earlier that thymidine kinase activity can be modulated by 5′-amino-dThd (5′-AdThd), as the natural dTTP does, affecting the cytotoxicity and metabolism of various dThd analogs used in the clinic as antineoplastic agents (29). 5′-AdThd was shown to antagonize dTTP feedback inhibition of TK and therefore to stimulate the anabolism of the anticancer drug 5-FdUrd (30). Thus, the use of compounds capable of antagonizing feedback inhibition of nucleoside analog activation (phosphorylation) may provide new means of increasing the efficacy of cytotoxic (anticancer) nucleoside analogs.

The α-CNPs might also have the intrinsic ability to target a wide variety of other (d)NTP-binding proteins, potentially also including G protein-coupled receptors (31), providing new opportunities in drug discovery. G protein-coupled receptors include a most diverse group of membrane receptors responsible for conducting many physiological processes through signal transduction, including intercellular communication, neuronal transmission, and hormonal signaling (32). They are also involved in a variety of pathological processes (31, 33) and are currently targets for at least one third of the pharmaceutical drug market (31).

The design of α-CNPs may also represent a technological tool for facilitating biochemical and structural studies of (d)NTP-binding proteins in the presence of α-CNPs as nonhydrolysable (d)NTP mimics. In fact, the nonhydrolysable ATP mimic adenosine 5′-(β,γ-methylene)triphosphate has been demonstrated to be instrumental for an improved crystallography of proteins that use ATP as one of their ligands and to obtain mechanistic insights in the role of ATP in enzyme interaction and catalysis (34, 35). Therefore, α-CNPs should be further investigated for their interaction with (d)ATP-, (d)CTP-, or (d)TTP-binding proteins from a crystallographic and mechanistic viewpoint.

None of the α-CNPs have shown so far any significant cytostatic or cytotoxic activity in cell culture at concentrations as high as 100 μM. However, one of the reasons may be the poor, if any, efficient cellular uptake of the α-CNPs due to their highly charged nature. Cellular uptake should therefore be enhanced by designing lipophilic prodrugs of the α-CNPs neutralizing the phosphonate charge, a strategy that is applied in the clinically used drugs adefovir dipivoxil (Hepsera), tenofovir disoproxil (Viread), and tenofovir alafenamide (36, 37). These attempts are currently ongoing in our laboratories. Although it should be recognized that α-CNP selectivity will be a challenge in terms of target specificity, structural optimization (fine-tuning) in the nucleobase, α-carboxy phosphonate, and/or the linker (pentose) portions of the molecules may address this issue, as already demonstrated for the acyclic α-CNPs that are shown to have a shifted selectivity from HIV-1 RT to herpetic DNA polymerases.

Methods

Detailed descriptions of the experimental set-ups and compound characterization are provided in *SI Appendix, SI Methods*. Inhibition of RTs by the α-CNPs was evaluated using the respective homopolymeric template/primers poly rA.dT, poly rI.dC, and poly rU.dA and their appropriate corresponding radiolabeled dNTP substrates (Table 1) or in the presence of T50A DNA template/5′-radiolabeled PI DNA primer and a fixed dNTP concentration (Fig. 1). The herpetic DNA polymerases and the cellular DNA polymerases used gapped calf thymus DNA as the template (Table 1), except for VZV DNA polymerase, where poly dA.poly dT was used. The X-ray diffraction data were obtained for the HIV-1 RT/dsDNA/T-α-CNP ternary complex that contained a template adenine base overhang to allow base-pairing with T-α-CNP (Fig. 2). Allosteric inhibition of viral and cellular thymidine kinases and cellular dCMPD by α-CNPs was performed in the presence of the natural substrates (dThd and dCMP, respectively) and dCTP (for the dCMPD assay) and analyzed by anion exchange HPLC (Fig. 3).

ACKNOWLEDGMENTS. We thank Lizette van Berckelaer and Kristien Minner for excellent technical assistance, CHESS for X-ray data collection, and Christiane Callebaut and MPharmSc Annelies Stevaert for dedicated editorial assistance. The research was supported by Grants PF 10/018 and GOA 10/14 from KU Leuven (University of Leuven) (to J.B.), from National Institutes of Health Grant P50 GM103368 and R37 AI027690 MERIT Award (to E.A.), the Science Foundation Ireland (05/PICA/B802) (to A.R.M.), and the Canadian Institutes of Health Research (CIHR) (to M.G.). M.G. is the recipient of a career award from the Fonds de la recherche en santé du Québec (FRSQ). J.A.B. is the recipient of a Doctoral Training Scholarship from FRSQ and a Chemical Biology Training Program Scholarship from CIHR.

1. Brautigam CA, Steitz TA (1998) Structural and functional insights provided by crystal structures of DNA polymerases and their substrate complexes. *Curr Opin Struct Biol* 8(1):54–63.
2. Steitz TA (1999) DNA polymerases: Structural diversity and common mechanisms. *J Biol Chem* 274(25):17395–17398.
3. Castro C, et al. (2009) Nucleic acid polymerases use a general acid for nucleotidyl transfer. *Nat Struct Mol Biol* 16(2):212–218.
4. Cowan JA (1998) Metal activation of enzymes in nucleic acid biochemistry. *Chem Rev* 98(3):1067–1088.
5. Rogolino D, Carcelli M, Sechi M, Neamati N (2012) Viral enzymes containing magnesium: Metal binding as a successful strategy in drug design. *Coord Chem Rev* 256(23-24):3063–3086.
6. Balzarini J, et al. (1993) Differential antiherpesvirus and antiretrovirus effects of the (S) and (R) enantiomers of acyclic nucleoside phosphonates: Potent and selective in vitro and in vivo antiretrovirus activities of (R)-9-(2-phosphonomethoxypropyl)-2,6-diaminopurine. *Antimicrob Agents Chemother* 37(2):332–338.
7. Balzarini J (1994) Metabolism and mechanism of antiretroviral action of purine and pyrimidine derivatives. *Pharm World Sci* 16(2):113–126.
8. Keane S, et al. (2015) Design and synthesis of alpha-carboxy nucleoside phosphonate (alpha-CNP) analogues and evaluation as HIV-1 reverse transcriptase-targeting agents. *J Org Chem,* 10.1021/jo502549y.
9. Allaudeen HS, Kozarich JW, Bertino JR, De Clercq E (1981) On the mechanism of selective inhibition of herpesvirus replication by (E)-5-(2-bromovinyl)-2′-deoxyuridine. *Proc Natl Acad Sci USA* 78(5):2698–2702.
10. Cheng YC, et al. (1981) Mode of action of phosphonoformate as an anti-herpes simplex virus agent. *Biochim Biophys Acta* 652(1):90–98.
11. Furman PA, et al. (1986) Phosphorylation of 3′-azido-3′-deoxythymidine and selective interaction of the 5′-triphosphate with human immunodeficiency virus reverse transcriptase. *Proc Natl Acad Sci USA* 83(21):8333–8337.
12. Jochmans D, et al. (2006) Indolopyridones inhibit human immunodeficiency virus reverse transcriptase with a novel mechanism of action. *J Virol* 80(24):12283–12292.
13. Pradère U, et al. (2012) Synthesis and antiviral evaluation of bis(POM) prodrugs of (E)-[4′-phosphono-but-2′-en-1′-yl]purine nucleosides. *Eur J Med Chem* 57:126–133.
14. Marchand B, Götte M (2003) Site-specific footprinting reveals differences in the translocation status of HIV-1 reverse transcriptase. Implications for polymerase translocation and drug resistance. *J Biol Chem* 278(37):35362–35372.
15. Marchand B, Tchesnokov EP, Götte M (2007) The pyrophosphate analogue foscarnet traps the pre-translocational state of HIV-1 reverse transcriptase in a Brownian ratchet model of polymerase translocation. *J Biol Chem* 282(5):3337–3346.
16. Das K, Martinez SE, Bauman JD, Arnold E (2012) HIV-1 reverse transcriptase complex with DNA and nevirapine reveals non-nucleoside inhibition mechanism. *Nat Struct Mol Biol* 19(2):253–259.
17. Ehteshami M, et al. (2008) Mutations M184V and Y115F in HIV-1 reverse transcriptase discriminate against "nucleotide-competing reverse transcriptase inhibitors". *J Biol Chem* 283(44):29904–29911.
18. Tisdale M, Kemp SD, Parry NR, Larder BA (1993) Rapid in vitro selection of human immunodeficiency virus type 1 resistant to 3′-thiacytidine inhibitors due to a mutation in the YMDD region of reverse transcriptase. *Proc Natl Acad Sci USA* 90(12):5653–5656.
19. Sarafianos SG, et al. (1999) Lamivudine (3TC) resistance in HIV-1 reverse transcriptase involves steric hindrance with beta-branched amino acids. *Proc Natl Acad Sci USA* 96(18):10027–10032.
20. Munch-Petersen B (2010) Enzymatic regulation of cytosolic thymidine kinase 1 and mitochondrial thymidine kinase 2: A mini review. *Nucleosides Nucleotides Nucleic Acids* 29(4-6):363–369.
21. Heinemann V, Schulz L, Issels RD, Wilmanns W (1998) Regulation of deoxycytidine kinase by deoxycytidine and deoxycytidine 5′ triphosphate in whole leukemia and tumor cells. *Adv Exp Med Biol* 431:249–253.
22. Maley GF, Lobo AP, Maley F (1993) Properties of an affinity-column-purified human deoxycytidylate deaminase. *Biochim Biophys Acta* 1162(1-2):161–170.
23. Nordlund P, Reichard P (2006) Ribonucleotide reductases. *Annu Rev Biochem* 75: 681–706.
24. Ji X, et al. (2013) Mechanism of allosteric activation of SAMHD1 by dGTP. *Nat Struct Mol Biol* 20(11):1304–1309.
25. Vazquez-Padua MA, Kunugi K, Fischer PH (1989) Enzyme regulatory site-directed drugs: Study of the interactions of 5′-amino-2′, 5′-dideoxythymidine (5′-AdThd) and thymidine triphosphate with thymidine kinase and the relationship to the stimulation of thymidine uptake by 5′-AdThd in 647V cells. *Mol Pharmacol* 35(1):98–104.
26. Welin M, et al. (2004) Structures of thymidine kinase 1 of human and mycoplasmic origin. *Proc Natl Acad Sci USA* 101(52):17970–17975.
27. Grant S (1998) Ara-C: Cellular and molecular pharmacology. *Adv Cancer Res* 72: 197–233.
28. Plunkett W, Huang P, Searcy CE, Gandhi V (1996) Gemcitabine: Preclinical pharmacology and mechanisms of action. *Semin Oncol* 23(5, Suppl 10):3–15.
29. Vázquez-Padua MA (1994) Modulation of thymidine kinase activity: A biochemical strategy to enhance the activation of antineoplastic drugs. *P R Health Sci J* 13(1): 19–23.
30. Vázquez-Padua MA, Risueno C, Fischer PH (1989) Regulation of the activation of fluorodeoxyuridine by substrate competition and feedback inhibition in 647V cells. *Cancer Res* 49(3):618–624.
31. Rominger DH, Cowan CL, Gowen-MacDonald W, Violin JD (2014) Biased ligands: Pathway validation for novel GPCR therapeutics. *Curr Opin Pharmacol* 16:108–115.
32. Rosenbaum DM, Rasmussen SG, Kobilka BK (2009) The structure and function of G-protein-coupled receptors. *Nature* 459(7245):356–363.
33. Thompson MD, Burnham WM, Cole DE (2005) The G protein-coupled receptors: Pharmacogenetics and disease. *Crit Rev Clin Lab Sci* 42(4):311–392.
34. Zhang Y, El Kouni MH, Ealick SE (2006) Structure of Toxoplasma gondii adenosine kinase in complex with an ATP analog at 1.1 angstroms resolution. *Acta Crystallogr D Biol Crystallogr* 62(Pt 2):140–145.
35. Agrawal A, et al. (2013) Mycobacterium tuberculosis DNA gyrase ATPase domain structures suggest a dissociative mechanism that explains how ATP hydrolysis is coupled to domain motion. *Biochem J* 456(2):263–273.
36. Pertusati F, Serpi M, McGuigan C (2012) Medicinal chemistry of nucleoside phosphonate prodrugs for antiviral therapy. *Antivir Chem Chemother* 22(5):181–203.
37. Pradere U, Garnier-Amblard EC, Coats SJ, Amblard F, Schinazi RF (2014) Synthesis of nucleoside phosphate and phosphonate prodrugs. *Chem Rev* 114(18):9154–9218.

SUPPORTING INFORMATION

Materials and Methods

Figs. S1 to S8

Tables S1 to S6

ONLINE METHODS

Reverse transcriptase, nucleic acids, and small molecules

HIV-1 reverse transcriptase was expressed and purified as described previously (1). Oligodeoxynucleotides were synthesized and purchased from Integrated DNA Technologies, Coralville, USA. The following sequences were used as templates: T50A, CCAATATTCACCATCAAGGCTTGACGTGACTTCACTCCACTATACCACTC; PBS36a, GTAACT-AGATATCCCTCAGACCCTTTTAGTCAGAAT; PBS36t, GTAACTAGAAATCCCTCAGACCCTTT-TAGTCAGAAT, PBS36c, GTAACTAGAGATCCCTCAGACCCTTTTAGTCAGAAT; PBS36g, GTAACTAGACATCCCTCAGACCCTTTTAGTCAGAAT; PPT57, CGTTGGGAGTGAATTAGCC-CTTCCAGTCCCCCCTTTTCTTTTAAAAAGTGGCTAAGA. Primer sequences used were: P1, GAGTGGTATAGTGGAGTGAA; 8a, TTCTGACTAAAAGGGTCTGAGGGAT; PPT+16, AAAGGGGGGACTGGAAGGGCTAATT. Deoxynucleotides were purchased from Integrated DNA Technologies.

Compound characterization data

T-α-CNP [cis-1-{4-[Carboxy(phosphono)methoxy]cyclopentan-1-yl}thymine]

White solid; mp 228–230 °C; ν_{max}/cm^{-1} (KBr) 3152 (NH), 3025 (CH), 1691 (C=O), 1405, 1273 (P=O), 1058; ^{1}H NMR (600 MHz, D_2O) δ: 1.53–1.62 (m, 0.5H), 1.62–1.75 (m, 2.5H), 1.76 (s, 3H), 1.80–1.98 (m, 2H), 2.24–2.31 (m, 1H), 3.92 (d, PCH, J_{PH} = 18.6, 0.5H), 3.95–4.02 (m, 1.5H), 4.73–4.84 (m, 1H), 7.70 (s, 0.5H), 7.72 (s, 0.5H); ^{13}C NMR (150.9 MHz, D_2O) δ: 11.4, 11.5, 29.1, 29.2, 29.5, 30.6, 36.6, 37.5, 54.6, 54.8, 77.5 (d, J_{PC} = 143.5), 78.2 (d, J_{PC} = 143.4), 79.9 (d, J_{PC} = 11.2), 80.6 (d, J_{PC} = 10.9), 111.3, 111.4, 140.3, 140.5, 152.57, 152.59, 166.6, 176.3, 176.5; ^{31}P NMR (121.5 MHz, $CDCl_3$) δ: 12.4,

12.6; HRMS (ES+): calcd for $C_{12}H_{18}N_2O_8P$ $(M + H)^+$ 349.0801, found 349.0804; MS (ES+) *m/z*: 349 $(M + H)^+$.

C- α-CNP [cis-1-{4-[Carboxy(phosphono)methoxy]cyclopentan-1-yl}cytosine]

White solid; mp > 250 °C; υ_{max}/cm^{-1} (KBr): 3432 (br, NH), 2966 (CH), 1723 (C=O), 1650, 1595 (C=C), 1490, 1399, 1286 (P=O), 1172 (C-N), 1087 (C-O); ^{1}H NMR (600 MHz, D_2O) δ: 1.52–1.60 (m, 0.5H), 1.60–1.72 (m, 2.5H), 1.81–1.92 (m, 1H), 1.93–2.01 (m, 1H), 2.19–2.31 (m, 1H), 3.88 (d, J_{PH} = 18.0, 0.5H), 3.91–3.95 (m, 0.5H), 3.92 (d, J_{PH} = 18.6, 0.5H), 3.96–4.00 (m, 0.5H), 4.82–4.90 (m, 1H), 5.915 (d, *J* = 7.2, 0.5H), 5.923 (d, *J* = 7.8, 0.5H), 7.96 (d, *J* = 7.2, 0.5H), 7.97 (d, *J* = 7.2, 0.5H); ^{13}C NMR (150 MHz, D_2O) δ: 29.4, 30.0, 30.3, 31.1, 36.6, 37.9, 55.3, 55.6, 77.7 (d, J_{PC} = 142.1,), 78.4 (d, J_{PC} = 141.4, 79.8 (d, J_{PC} = 11.5), 80.5 (d, J_{PC} = 11.8), 96.30, 96.34, 144.7, 144.8, 158.42, 158.45, 165.35, 165.37, 176.8, 177.1; ^{31}P NMR (121.5 MHz, D_2O) δ: 11.3, 11.5; HRMS (ES+): calcd for $C_{11}H_{17}N_3O_7P$ $(M + H)^+$ 334.0804, found: 334.0802; MS (ES–) *m/z*: 332.0 $(M – H)^–$.

A- α-CNP [cis-9-{4-[Carboxy(phosphono)methoxy]cyclopentan-1-yl}adenine]

White solid; mp 236–240 °C; ν_{max}/cm^{-1} (KBr) 3342 (NH), 3198, 2961 (CH), 1603 (C=O), 1396, 1176 (C-N), 1071 (C-O); ^{1}H NMR (600 MHz, D_2O) δ: 1.86–2.23 (m, 5H), 2.55–2.64 (m, 1H), 3.91 (d, J_{PH} = 16.8, 0.55H), 3.96 (d, J_{PC} = 16.8, 0.45H), 4.09–4.17 (m, 1H), 4.75–4.83 (m [partially obscured by water], 1H), 8.11 (s, 0.45H,), 8.12 (s, 0.55H), 8.45 (s, 0.45H), 8.50 (s, 0.55H); ^{13}C NMR (150 MHz, D_2O) δ: 29.3, 30.5, 30.6, 30.7, 37.5, 38.6, 53.6, 53.8, 77.4 (d, J_{PC} = 145.9), 78.1 (d, J_{PC} = 148.8), 79.9 (d, J_{PC} = 10.3), 80.5 (d, J_{PC} = 10.7), 117.8, 117.9, 141.11, 141.14, 148.2, 151.2, 154.5, 154.6, 176.6, 176.8; ^{31}P NMR (121.5 MHz, D_2O) δ: 11.7, 11.8; HRMS (ES+): calcd for $C_{12}H_{17}N_5O_6P$ $(M + H)^+$ 358.0916, found 358.0898; MS (ES–) *m/z*: $(M – H)^–$

Acyclic T-butenyl- α-CNP [cis-2-(4-(2,4-Dioxo-5-methyl-pyrimidin-1-yl)but-2-enyloxy)-2-phosphonoacetic acid]

White solid; δ_H (300 MHz, D_2O): 1.78 (s, 3H), 3.84-3.90 (d, 1H, J_{PH}= 18.6 Hz), 4.02-4.19 (m, 2H), 4.35-4.37 (m, 2H), 5.49-5.58 (m, 1H), 5.79-5.82 (m, 1H), 7.41 (s, 1H) ppm; δ_C (75 MHz, D_2O): 11.2, 45.4,

66.3, 66.5, 79.8, 81.6, 110.9, 126.5, 130.7, 142.8, 152.3, 167.1, 177.4 ppm; δ_P (160 MHz, $CDCl_3$): 12.3-12.4 (d, *J*= 17 Hz) ppm; LRMS (ESI) mass calculated for $C_{11}H_{15}N_2O_8P$ $(M+H)^+$ 335.1; Found: 335.4.

DNA synthesis

A 3-fold excess of T50A DNA template was heat-annealed to 50 nM 5'-radiolabeled P1 DNA primer, then incubated with 250 nM of RT in a buffer containing 50 mM Tris-HCl pH 7.8, 50 mM NaCl, 0.3 mM EDTA, and 0.5 µM of each of dATP, dTTP, dGTP, and dCTP (1). The samples were preincubated at 37°C for 5 minutes before starting the reactions. In the time course experiment, samples were treated with either no inhibitor, or 200 µM of T-α-CNP, C-α-CNP, or A-α-CNP; the reactions were initiated with 6 mM $MgCl_2$ and allowed to proceed for up to 30 minutes. For inhibitor dose-response experiments, each of the three inhibitors was titrated up to 200 µM, and the reaction was initiated with 6 mM $MgCl_2$ and allowed to proceed for 3 minutes. For both types of experiments, the reaction was stopped with 100% formamide loading dye containing traces of xylene cyanol and bromophenol blue. Samples were resolved on a 12% denaturing polyacrylamide gel followed by phosphorimaging (Amersham Biosciences). For the dose-response experiments, pausing sites caused by inhibition were quantified and summed; the % inhibition was calculated as the total amount of inhibited product divided by the amount of full-length product plus inhibition products, multiplied by 100. The product fractions were normalized and plotted against inhibitor concentration using GraphPad Prism software; the normalized data was fitted to a *log[inhibitor] versus response* curve with variable slope to extract IC_{50} values for the inhibition of WT and mutant RT enzymes by the α-CNP.

Electrophoretic mobility shift assay (EMSA)

Ternary complex formation was monitored using 50 nM of a 5' radiolabeled primer (8a) annealed to a three-fold molar excess of one of four templates (PBS36/a/t/c/g). The DNA hybrid was incubated with 500 nM WT HIV-1 RT in a buffer containing 50 mM Tris-HCl pH 7.8 and 6 mM $MgCl_2$ in a final volume of 25 µL. Serial dilutions of C-α-CNP were added to the sample set and the tubes were incubated for 10 min at 25°C. Challenge of complexes was performed by addition of 4 µg/µl heparin, and subsequent incubation for 30 minutes at 25°C. Five µL of a solution containing 50% sucrose and a

trace of bromophenol blue was then added to the samples. Complexes were subjected to 6% non-denaturing polyacrylamide electrophoresis and analyzed by phosphorimaging.

Site-specific footprinting

Chemical footprinting with Fe^{2+} of the template strand was conducted using 50 nM 5'-radiolabeled DNA template (PPT-57) annealed to 150 nM of the primer (PPT+16). The hybrid was incubated with 750 nM HIV-1 RT in a buffer containing 120 mM sodium cacodylate (pH 7), 20 mM NaCl, and 6 mM $MgCl_2$ in a final volume of 50 µL. Increasing concentrations of C-α-CNP were added to the samples; control lanes using the prototype translocational inhibitors PFA (PRE) and INDOPY-1 (POST) were included, in addition to samples without inhibitor and without Fe^{2+} treatment. Pre-incubation of complexes at 37°C for 10 minutes was performed prior to the treatment with Fe^{2+}. Treatment with Fe^{2+} was performed as previously described (2).

Reverse transcriptase assay with homopolymeric template/primers

HIV-I RT assays were also carried out in the presence of artificial homopolymeric template/primers. Poly(A), dT_{12-18}, dC_{12-18}, poly(I), dA_{12-18} and poly(U) were from Pharmacia (Uppsala, Sweden). To prepare the template/primers for the RT experiments, 0.15 mM poly(U), poly(A), and poly(I) were mixed with an equal volume of 0.0375 mM oligo(dA), oligo(dT), and oligo(dC), respectively. The reaction mixture (50 µl) contained 50 mM Tris.HC1 pH 7.8, 5 mM dithiothreitol, 300 mM glutathione, 500 µM EDTA, 150 mM KCl, 5 mM $MgCl_2$, 1.25 µg of bovine serum albumin, an appropriate concentration of the tritium-labeled substrate [CH_3-^{3}H]dTTP, [5-^{3}H]dCTP, or [2,8-^{3}H]dATP (2 µCi/assay), a fixed concentration of the template/primer poly(A).oligo(dT) (0.015 mM), poly(I).oligo(dC) (0.015 mM), or poly(U).oligo(dA) (0.015 mM), 0.06% Triton X-100, 10 µl of α-CNP inhibitor solution (containing various concentrations of the compounds), and 1 µl of the HIV-1 RT preparation. The reaction mixtures were incubated at 37°C for 30 minutes, at which time 100 µl of calf thymus DNA (150 µg/ml), 2 ml of $Na_4P_20_7$ (0.1 M in 1 M HCl), and 2 ml of trichloroacetic acid (10% v/v) were added. The solutions were kept on ice for 30 minutes, after which the acid-insoluble material was washed and analyzed for radioactivity. For the experiments in which the 50% inhibitory

concentration (IC_{50}) of the test compounds was determined, fixed concentrations of 1.25 µM [^{3}H]dTTP, 1.75µM [^{3}H]dATP, or 2.5 µM [^{3}H]dCTP were used. In the assays in which the IC_{50} and K_i values of the test compounds were determined with respect to the template/primers, appropriate concentrations of template/primer were used. For the experiments in which the K_i values of the test compounds were determined with respect to the template/primers, appropriate concentrations of the template/primers were used in the presence of a fixed concentration of 1.25 µM [^{3}H]dTTP, 1.75 µM [^{3}H]dATP, and 2.5 µM [^{3}H]dCTP.

Enzyme assay with HCMV DNA polymerase

The pGEM3Z-CMV UL54 plasmid for expression of the catalytic subunit (UL54 protein) of HCMV DNA polymerase was a generous gift from T. Cihlar (Gilead Sciences, Foster City, CA) (3). Protein expression was performed with the TnT® SP6 Quick Coupled Transcription/Translation System (Promega) (4). The plasmid was added (at 10 ng per µl volume) to the TnT® mix containing 0.5 mM $MgCl_2$ and 10 mM potassium acetate, and the mixture was incubated for 3 hours at 30°C. To perform the HCMV DNA polymerase assay, 4 µl of the TnT® reaction product was added to a 46 µl mixture to obtain 25 mM Tris.HCl pH 8.0, 100 mM $(NH_4)_2SO_4$, 0.5 mM dithiothreitol, 10 mM $MgCl_2$, 0.2 mg/ml bovine serum albumin, 5 % glycerol, 150 ng per µl activated calf thymus DNA (from Amersham Biosciences, Piscataway, N.J.), 100 µM of each of the three unlabeled dNTPs, and 0.5 µM of the rate-limiting tritium-labeled dNTP, and serial dilutions of the L-enantiomeric α-CNPs. Foscarnet was included as the reference compound. After 60 minutes incubation at 37°C, nucleic acids were precipitated by addition of 1 ml of ice-cold 5% TCA and 20 mM $Na_4P_2O_7$, then spotted onto glass microfiber filters (type G/C; GE Health Care UK Limited, Buckinghamshire, UK) and further washed with 5% TCA and ethanol to remove free radiolabeled dNTP. Radioactivity was determined in a Packard (Perkin Elmer, Zaventem, Belgium) Tri-Carb 2300 TR liquid scintillation counter. All radiolabeled materials were obtained from Moravek (Brea, CA).

Enzyme assay with herpes simplex virus type 1 (HSV-1) DNA polymerase and cellular DNA polymerases α and β

The reaction mixture (40 µl) for the HSV-1 DNA polymerase and cellular DNA polymerase α assays contained 4 µl of Premix (200 mM Tris.HCl pH 7.5; 2 mM DTT; 30 mM $MgCl_2$), 4 µl of BSA (5 mg/ml), 1.6 µl of activated calf thymus DNA (1.0 mg/ml), 0.8 µl of dCTP (5 mM), 0.8 µl of dATP (5 mM), 0.8 µl of dGTP (5 mM), 2 µl of radiolabeled [3H]dTTP (1 mCi/ml) (3.2 µM), 18 µl of H_2O, and 4 µl of T-α-CNP at different serial concentrations (i.e., 200, 40, 8, 1.6, 0.32 µM). For testing the C-α-CNP analogue, 2 µl [^{3}H]dCTP (1 mCi/ml) and 0.8 µl unlabelled dTTP, dATP, and dGTP (5 mM) were used. For testing the A-α-CNP analogue, 2 µl [^{3}H]dATP (1 mCi/ml) and 0.8 µl unlabeled dTTP, dCTP and dGTP (5 mM) were used. The reaction was started by the addition of 4 µl of recombinant HSV-1 DNA polymerase (kindly provided by M.W. Wathen, at that time at Pfizer, Kalamazoo, MI) or human cellular DNA polymerase α or β (Chimerix, Milwaukee, WI) (in 20 mM Tris.HCl pH 8.0; 1 mM DTT; 0.1 mM EDTA; 0.2 M NaCl; 40% glycerol), and the reaction mixture was incubated for 60 minutes at 37°C. Then, 1 ml of ice-cold 5% TCA in 0.02 M $Na_4P_2O_7$.10 H_2O was added to terminate the polymerization reaction. The consecutive steps (i.e. capture of the acid-insoluble precipitate onto filters, filter washing and scintillation counting) were done as described above.

Enzyme assay with varicella-zoster virus (VZV) DNA polymerase

The VZV DNA polymerase assay was as follows: the 50 µl-reaction mixture contained 6.4 mM HEPES, 12 mM KCl, 25 mM NaCl, 5 mM $MgCl_2$, 4.6 µg BSA, 2 mM CHAPS, 5 mM DTT, 5% glycerol, 1 µCi [^{3}H]dTTP, 100 µM poly dA.oligo dT, and 5 µl of serial dilutions of T-α-CNP. The reaction was started by the addition (5 µl) of recombinant VZV DNA polymerase (kindly provided by M.W. Wathen) in 5 mM HEPES and incubated for 60 min at 37°C. The termination of the enzyme reaction and all consecutive steps to quantify the [^{3}H]dTTP incorporation into the template/primer were done as described above.

X-ray crystallography

HIV-1 RT for the structural study was expressed, purified, and cross-linked to a dsDNA template/primer using a previously described protocol (5). A 27-mer template (5'-

ATGGACGGCGCCCGAACAGGGACTGTG-3') and a 20-mer primer (5'-ACAGTCCCTGTTCGGsCGCC-3') were used for cross-linking with RT (5). The primer was extended by catalytic incorporation of a ddGMP at the 3'-end of the primer by RT while crosslinking the template/primer at the Q258C position. The complex was purified and crystallized using a previously described protocol (5). The crystals were soaked with 2 mM T-α-CNP in the presence of 20 mM $MgCl_2$ to obtain an RT/dsDNA/T-α-CNP ternary complex. The X-ray diffraction data for the complex was collected from one flash-frozen crystal at the CHESS F1 beamline. The structure was solved by molecular replacement using the protein model from the RT/dsDNA/AZT-TP structure (PDB ID 3V4I). The position and conformation of T-α-CNP was defined by difference electron density. The final model of RT/dsDNA/T-α-CNP complex was refined at 2.9 Å resolution to an R and R-free of 0.199 and 0.251. The crystallographic software packages HKL2000, Phenix, and Coot were used for data processing, structure refinement, and model building, respectively. The diffraction data and refinement statistics are summarized in Table S3, and the structure is deposited in the Protein Data Bank (PDB) with accession number 4R5P.

Thymidine kinase assay

The assay was performed as follows: The recombinant cytosolic thymidine kinase (TK-1), mitochondrial TK-2, HSV-1 TK, and VZV TK were incubated at 37°C for 30 min in the presence of different concentrations of the test compounds T-α-CNP, C-α-CNP, A-α-CNP and dTTP in a 50-µl-reaction mixture containing 50 mM Tris-HCl (pH 8.0), 2.5 mM $MgCl_2$, 10 mM dithiothreitol, 0.5 mM CHAPS, 3 mg/ml bovine serum albumin, 2.5 mM ATP, and a variety of different concentrations of [methyl-^{3}H]deoxythymidine ([methyl-^{3}H]dThd). After the incubation time, 45-µl aliquots of the reaction mixtures were spotted on Whatman DE-81 (anion exchange) filter paper disks. The filters were washed three times for 5 min in 1 mM ammonium formate, once for 1 min in water, and once for 5 min in ethanol. The radioactivity was determined by scintillation counting.

dCMP deaminase assay

The effect of C-α-CNP on the activity of recombinant human dCMP-deaminase (dCMPD; Prospec, NJ) was evaluated. Deamination of dCMP (25, 50, 75, and 100 µM) by dCMPD (250 pg/µL) was assayed in 100 µL of 50 mM Tris.HCl pH 7.5, containing different concentrations of C-α-CNP (625, 250, 125, and 0 µM), dCTP (250 µM), $MgCl_2$ (5 mM), and DMSO (5%). After 10 min incubation at 37°C, the reaction was stopped by the addition of 200 µL ice-cold MeOH. Samples were kept on ice for 10 min and subsequently cleared by centrifugation at 16,000 x g for 15 min. The supernatant was analyzed by HPLC (Alliance 2690; Waters, Milford, MA) using a Partisphere-SAX anion exchange column (5.6 x 125 mm, Whatman International Ltd., Maidstone, UK). The following gradient was used to separate dCMP (RT = 4.2 min) from dUMP (RT = 7.4 min): 5 min at 100% buffer B (5 mM $NH_4H_2PO_4$ pH 5); a 15 min linear gradient of 100% buffer B to 100% buffer C (300 mM $NH_4H_2PO_4$ pH 5); 10 min at 100% buffer C; a 5 min linear gradient to 100% buffer B; equilibration at 100% buffer B for 5 min.

CMP/UMP kinase assay

The reaction mixture (300 µl) consisted of reaction buffer (Tris.HCl 50 mM, $MgCl_2$ 5 mM, pH 7.5) to which was added 100 µM U-α-CNP or C-α-CNP, or 100 µM of the natural substrates UMP or CMP (included as reaction substrate controls), 5 mM ATP as phosphate donor, and recombinant CMP/UMP kinase (6) to initiate the CMP/UMP kinase reaction at 37°C. At 0, 15, 30, 120 min and 24 hr, 100 µl of the reaction mixture was withdrawn, added to 200 µl ice-cold methanol and kept on ice for 10 min. Then, the methanol-insoluble material was removed by centrifugation and the supernatant subjected to HPLC analysis on a Partisyl SAX column (Hichrom (125 x 4.6 mm), Reading, Berkshire, UK) to separate and quantify the reaction products.

NDP kinase assay

The reaction mixture (400 µl) consisted of phosphate-buffered saline (PBS) containing 100 µM of T-α-CNP, C-α-CNP or A-α-CNP, or 200 µl of the natural substrates dTDP, CDP or ADP (included as reaction controls), 200 µM ATP as phosphate donor, 1 mM $MgCl_2$ and recombinant NDPK (Sigma-Aldrich, St. Louis, Mo) to initiate the NDPK reaction at 37°C. At 0, 30 and 60 min, 100 µl of the reaction mixture was withdrawn, added to 200 µl ice-cold methanol and kept on ice for 10 min. Then,

the methanol-insoluble material was removed by centrifugation and the supernatant subjected to HPLC analysis on a Partisyl SAX column to separate and quantify the reaction products.

Cellular assays

The antiproliferative (cytostatic) activity determination of the α-CNPs was performed as follows: to each well of a 96-well microtiter plate were added an appropriate amount of human $CD4^+$ T-lymphocyte CEM or cervix carcinoma HeLa cells and a 5-fold dilution series of the test compounds (highest concentration tested: 200 μM). The cells were allowed to proliferate for 72 hr (CEM) or 96 hr (HeLa) at 37°C in a humidified CO_2-controlled atmosphere. At the end of the incubation period, the cells were counted in a Coulter counter (Coulter Electronics Ltd., Harpenden, Herts, UK).

The cytotoxic activity determination of the α-CNPs was performed as follows: confluent (human lung fibroblast HEL or cervix carcinoma HeLa) cell cultures in 96-well microtiter wells were exposed to a 5-fold dilution series of the test compounds (highest concentration tested: 200 μM). After a 3 day incubation period at 37°C, microscopically visible alteration of cell morphology was examined.

The antiherpes virus [herpes simplex virus type 1 (HSV-1) (KOS); HSV-2 (G)] assays were based on inhibition of virus-induced cytopathicity in HEL cell cultures. Confluent HEL cell cultures in microtiter 96-well plates were inoculated with 100 $CCID_{50}$ of virus (1 $CCID_{50}$ being the virus dose to infect 50% of the cell cultures). The cell cultures were incubated at the time of infection in the presence of varying concentrations (200, 40, 8, 1.6 and 0.32 μM) of the test compounds. Viral cytopathicity was recorded microscopically as soon as it reached completion in the control virus-infected cell cultures that were not treated with the test compounds. The methodology of the anti-HIV assays was as follows: human CEM cells (~ 3×10^5 cells/mL) were infected with 100 $CCID_{50}$ of HIV(III_B) or HIV-2(ROD)/mL and seeded in 200-μL wells of a microtiter plate containing appropriate dilutions of the test compounds. After 4 days of incubation at 37 °C, HIV-induced giant cell formation was examined microscopically.

Kinetical analysis

The nature of the kinetic interaction of the T-α-CNP, AZTTP, and INDOPY-1 against HIV-1 RT and T-α-CNP and dTTP against dThd kinase were analysed by the mixed model using a non-linear regression method available in GraphPad. The mixed model uses a general equation including competitive, uncompetitive and noncompetitive inhibition as special cases. Following equations were used: $V_{max(app)} = V_{max}/[1+I/\alpha Ki]$; $K_{m(app)} = K_m.[1+I/K_i]/[1+I/\alpha Ki]$; $Y = V_{max(app)}.X/[K_{m(app)}+X]$, in which X is substrate concentration; Y is enzyme activity; V_{max} is maximum enzyme velocity; K_m = Michaelis-Menten constant; I is inhibitor concentration; K_i = inhibition constant and α is a constant that determines the kinetic mechanism. When α = 1, kinetics are noncompetitive. When α is very large, the kinetic model approaches a competitive interaction; when α is very small (but greater than zero), the kinetic model approaches an uncompetitive interaction. The R^2-value represents a parameter for the goodness of curve fit.

References

1. Le Grice SF, Gruninger-Leitch F (1990) Rapid purification of homodimer and heterodimer HIV-1 reverse transcriptase by metal chelate affinity chromatography. *Eur J Biochem/FEBS* 187:307-314.
2. Marchand B, Götte M (2003) Site-specific footprinting reveals differences in the translocation status of HIV-1 reverse transcriptase. Implications for polymerase translocation and drug resistance. *J Biol Chem* 278:35362-35372.
3. Cihlar T, Fuller MD, Cherrington JM (1997) Expression of the catalytic subunit (UL54) and the accessory protein (UL44) of human cytomegalovirus DNA polymerase in a coupled in vitro transcription/translation system. *Protein Expr Purif* 11:209-218.
4. De Bolle L, Manichanh C, Agut H, De Clercq E, Naesens L (2004) Human herpesvirus 6 DNA polymerase: enzymatic parameters, sensitivity to ganciclovir and determination of the role of the A961V mutation in HHV-6 ganciclovir resistance. *Antiviral Res* 64:17-25.

5. Sarafianos SG, et al. (1999) Lamivudine (3TC) resistance in HIV-1 reverse transcriptase involves steric hindrance with beta-branched amino acids. *Proc Natl Acad Sci USA* 96:10027-10032.
6. Van Rompay AR, Johansson M, Karlsson A (1999) Phosphorylation of deoxycytidine analog monophosphates by UMP-CMP kinase: molecular characterization of the human enzyme. *Mol Pharmacol* 56:562-569.

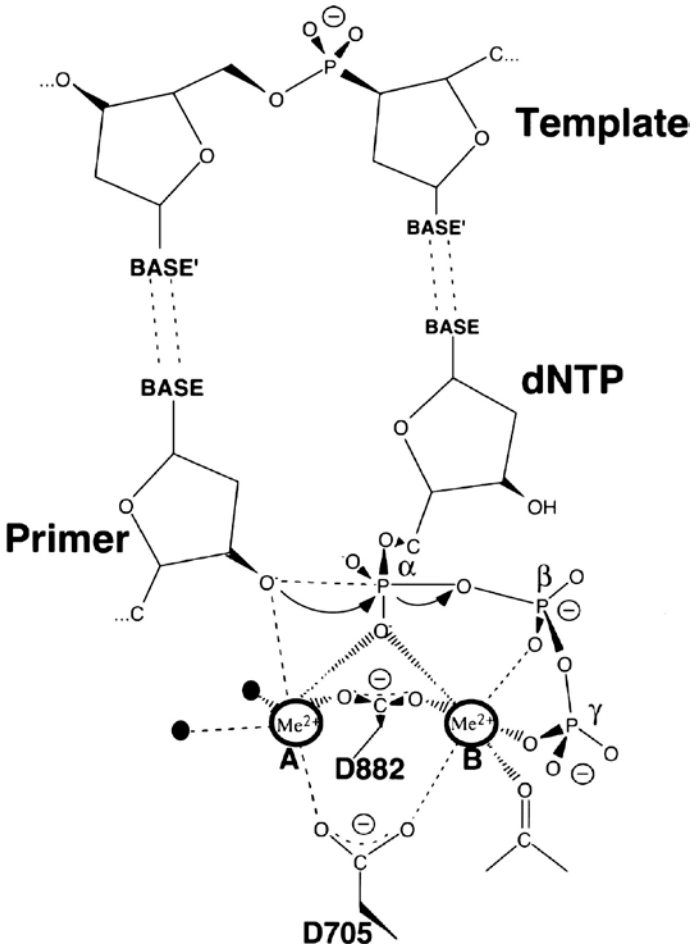

Fig. S1. The two-metal ion mechanism of DNA polymerase. The two conserved aspartates D705 and D882 have the *E. coli* DNA polymerase I numbering. The DNA polymerase active site features two metal cations that stabilize the transition state. Metal ion A activates the primer 3'-OH for a nucleophilic attack on the α-phosphate of the dNTP. Metal ion B plays the dual role of stabilizing the negative charge that builds up on the leaving oxygen and chelating one oxygen from each of the α-, β-, and γ-phosphates. Metal B helps to orient the phosphates appropriately for polymerization and facilitates the release of pyrophosphate, the catalytic reaction byproduct. The filled circles represent water molecules. This configuration also supports an extended version of this model that considers simultaneous deprotonation of the 3'-OH of the primer and protonation of the pyrophosphate leaving group (1). The figure is taken from Steitz (2).

1. Castro C, et al. (2009) Nucleic acid polymerases use a general acid for nucleotidyl transfer. *Nat Struct Mol Biol* 16:212-218.

2. Steitz TA (1999) DNA polymerases: structural diversity and common mechanisms. *J Biol Chem* 274:17395-17398.

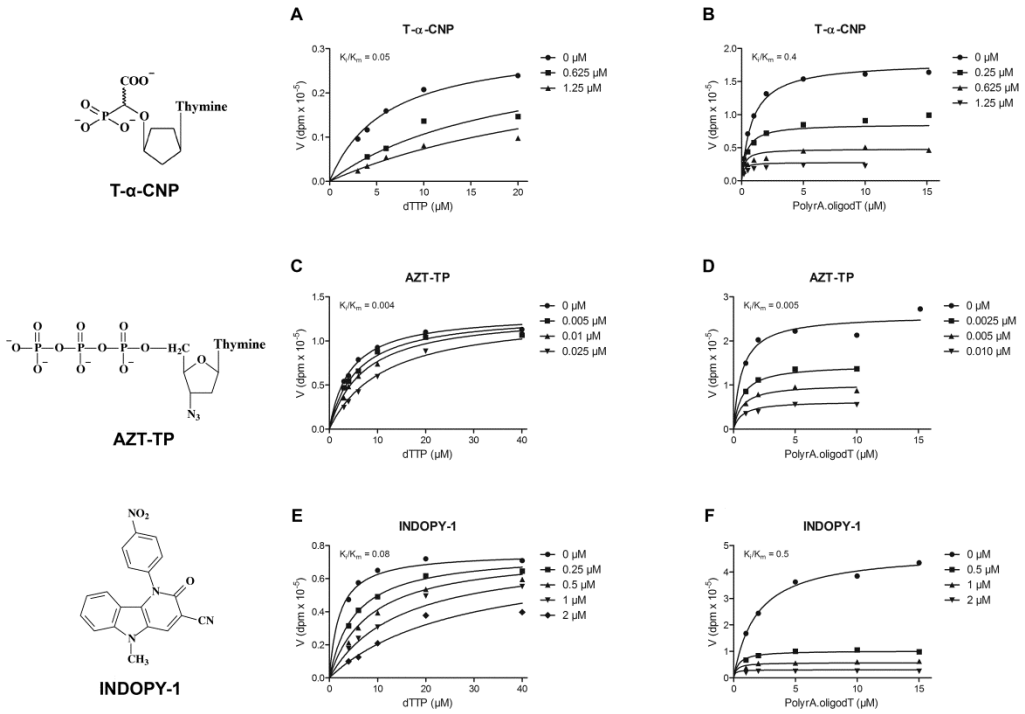

Fig. S2. Kinetic plot analyses for inhibition of HIV-1 RT by T-α-CNP (panels *A*, *B*), the NRTI AZT-TP (panels *C*, *D*) and the NcRTI INDOPY-1 (panels *E*, *F*). Test compounds were evaluated in the presence of varying concentrations of radiolabeled [CH_3-^{3}H]dTTP substrate and a fixed template/primer poly rA.oligo dT concentration (panels *A*, *C*, *E*) or in the presence of varying concentrations of template/primer (poly rA.dT) and a fixed [CH_3-^{3}H]dTTP concentration (panels *B*, *D*, *F*). The kinetics are competitive-type for T-α-CNP, AZT-TP and INDOPY-1 in the presence of variable dTTP substrate concentrations. The kinetics are non-competitive-type for AZT-TP and close to uncompetitive-type for T-α-CNP and INDOPY-1 in the presence of variable template/primer concentrations. The data were analyzed using the mixed model inhibition of GraphPad (Table S2).

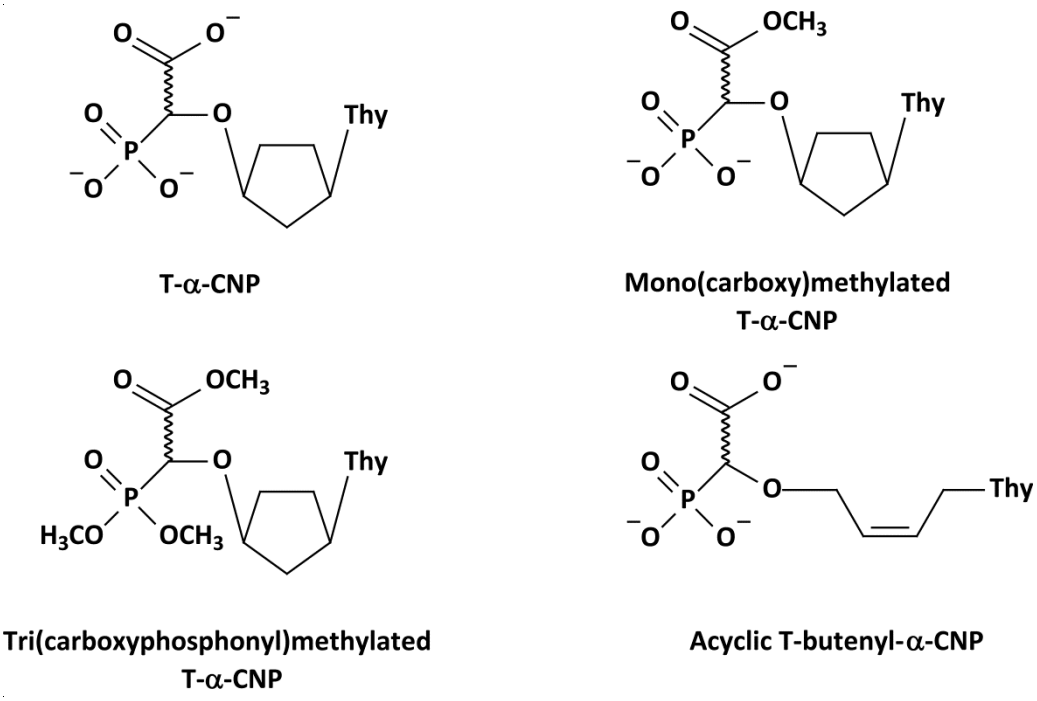

Fig. S3. Structural formulas of T-α-CNP, methylated T-α-CNPs and the acyclic T-butenyl-α-CNP. Methylated T-α-CNPs were evaluated as their D/L-enantiomeric mixtures (1:1).

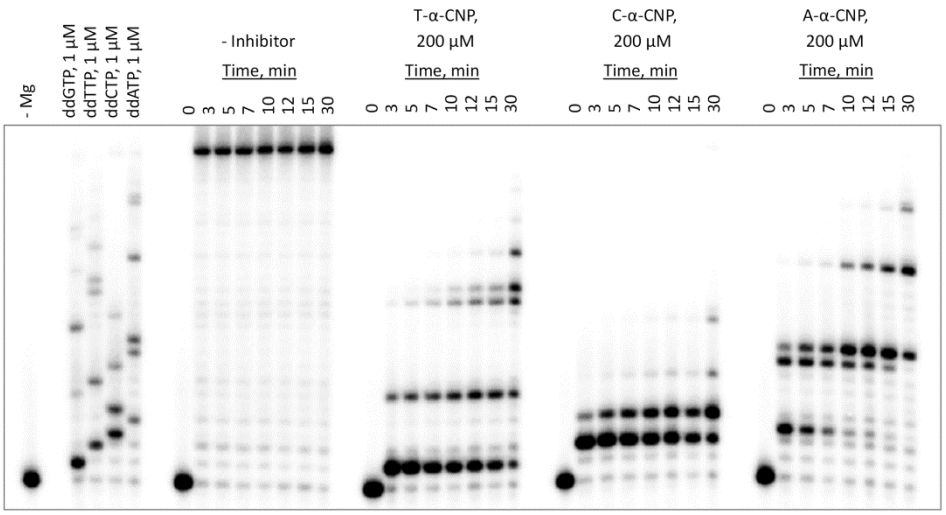

Figure S4 Inhibition of DNA synthesis monitored in *time-course experiments* at different fixed dNTP concentrations, T50A DNA template/5'-radiolabeled P1 DNA primer and a fixed concentration of T-, C-, and A-α-CNP, respectively. Strong and specific sites of inhibition (short oligonucleotide sequences) disappear over time, while other specific sites of inhibition (longer oligonucleotide sequences) appear over time (last three lane series). The second left lane series shows control reactions taken at different time points in the absence of α-CNPs. The most left lane series shows control reactions with the obligate DNA chain-terminating nucleotides ddGTP, ddTTP, ddCTP and ddATP.

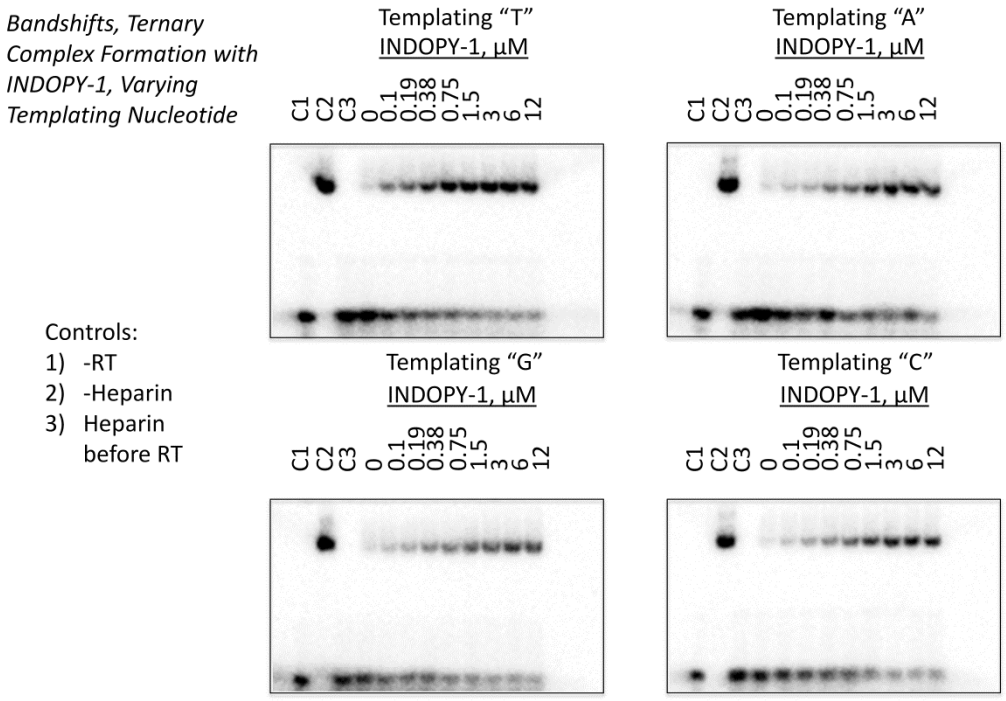

Fig. S5. Ternary RT-template/primer-inhibitor complex formation in the presence of INDOPY-1. Specific INDOPY-1 binding to HIV-1 RT was analyzed with four different template/primer combinations that contain either a thymine, adenine, guanine, or cytosine nucleotide, downstream of the 3'-end of the primer. Complex formation with HIV-1 RT was monitored with increasing concentrations of INDOPY-1. Stable, heparin-resistant ternary complexes are observed in the presence of INDOPY-1, irrespective of the templating nucleobase.

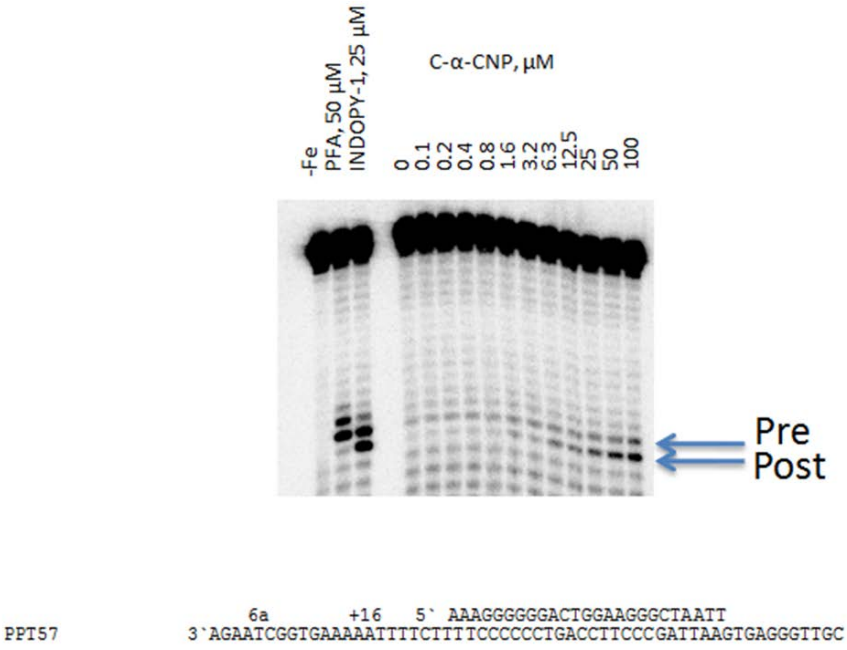

Fig. S6. Site-specific footprinting for α-CNP interaction with HIV-1 RT and the template/primer. The precise position of HIV-1 RT on its template/primer was analyzed through Fe^{2+}-mediated footprinting. Upon binding of the Fe^{2+} ion to the RNase H domain, the template is cut in a site-specific manner that enables the distinction between pre- and post-translocated complexes. Like the prototype NcRTI (INDOPY-1), increasing concentrations of C-α-CNP trap the HIV-1 RT as a post-translocated complex. Concentrations of approximately 6 µM of C-α-CNP were required to trap 50% of the complexed enzyme populations in the post-translocational state.

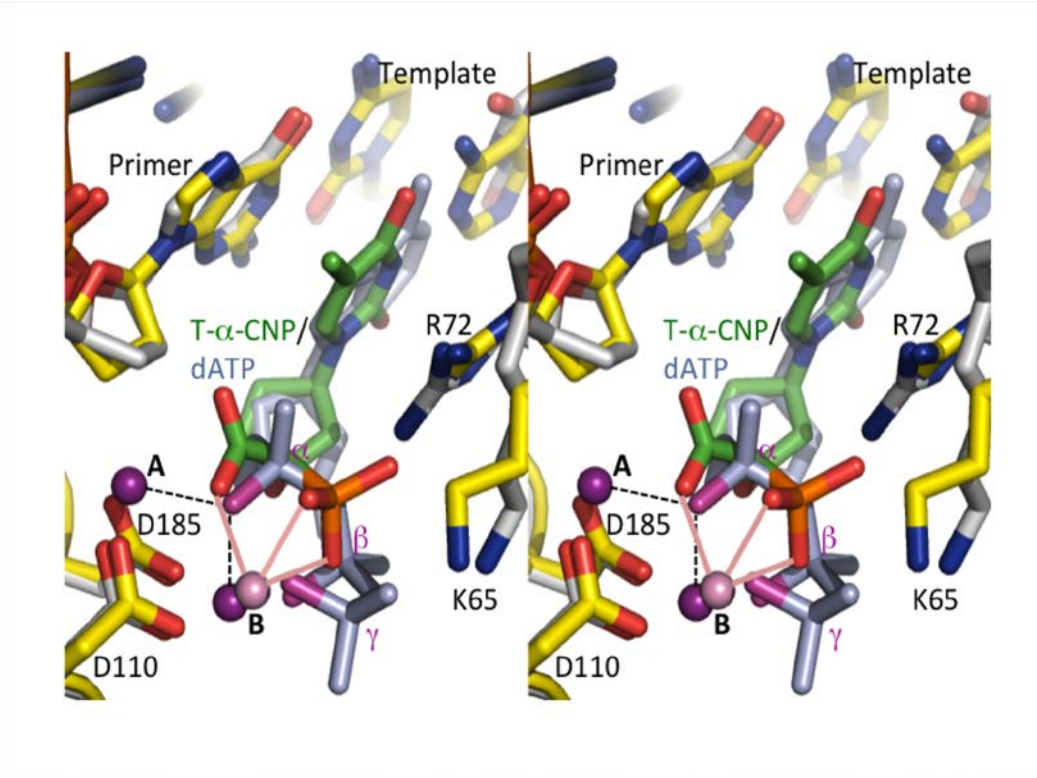

Fig. S7. Stereo view of the molecular interaction of T-α-CNP with HIV-1 reverse transcriptase. Superposition of RT/RNA-DNA/dATP structure (PDB ID 4PQU; in gray scale) on RT/dsDNA/T-α-CNP (yellow protein/DNA and green T-α-CNP) structure. Both the complexes were crystallized in similar condition and crystal lattice, and 2.51 Å structure 4PQU has both the catalytic Mg^{2+} ions (purple) present at the polymerase active site. The chelating oxygen atoms of α-, β-, and γ-phosphates are colored purple. Highly analogous chemical and geometrical environments at the polymerase active sites in both the structures suggest that like a dNTP, T-α-CNP binding to RT involves chelation to both the Mg^{2+} ions; the metal A is not observed in most of RT/dsDNA/dNTP (or analog) structures, due to presumably the missing 3'-OH at the DNA primer terminus. The base-pairing, base stacking, and metal chelation interactions are conserved between T-α-CNP and a dNTP when bound to RT; however, the residue K65 that interacts with the γ-phosphate of dNTP is located away from T-α-CNP. The template/primer was designed to have an adenine nucleobase overhang for base-pairing with T-α-CNP.

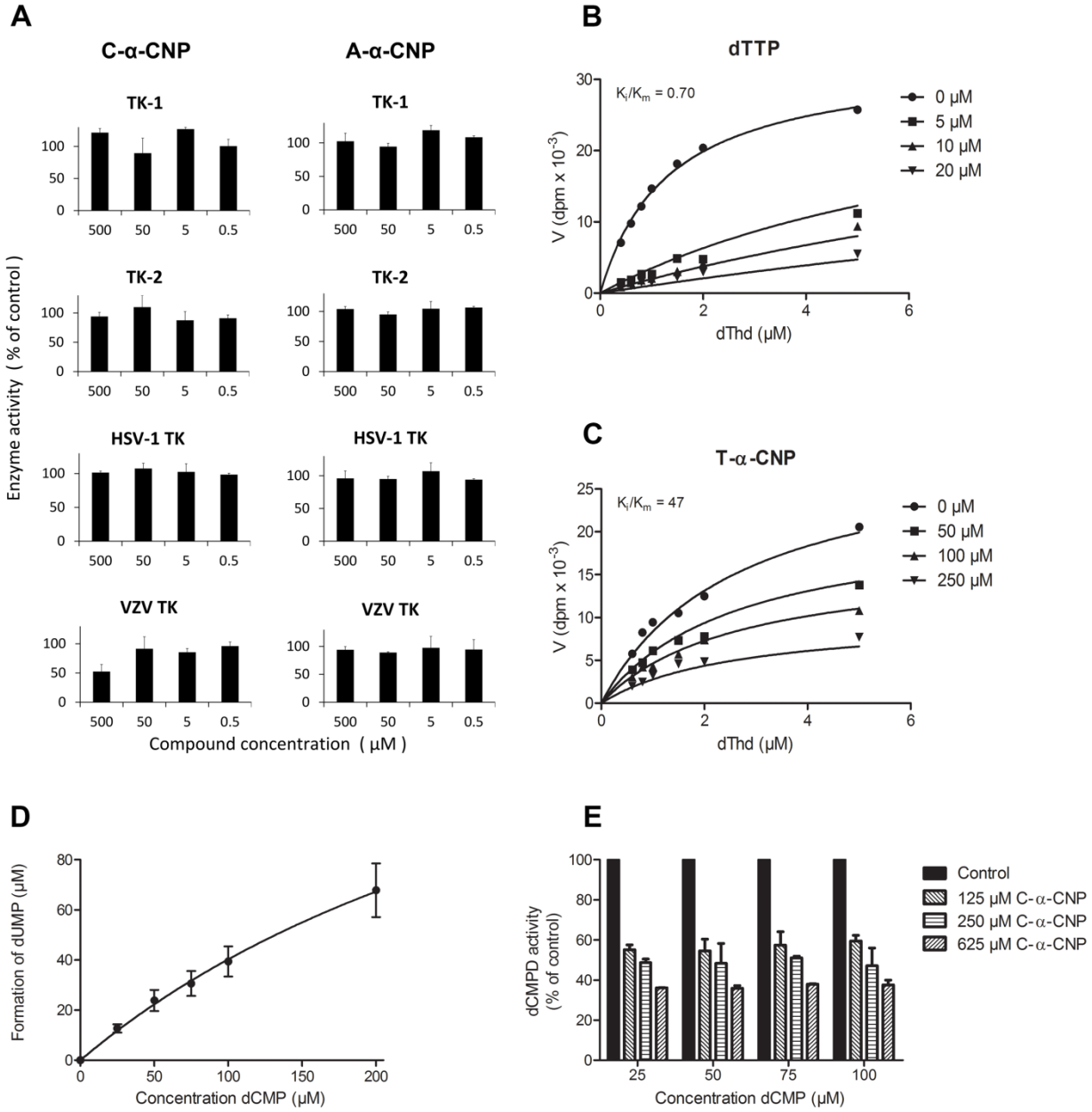

Fig. S8. Allosteric inhibition of thymidine kinase (TK) and 2'-deoxycytidylate deaminase (dCMPD) by α-CNP. Panel *A*. Exposure of the L-enantiomeric C- and A-α-CNPs to cytosolic TK-1, mitochondrial TK-2, herpes simplex virus type 1 TK, and varicella-zoster virus TK at varying α-CNP concentrations. Panels *B* and *C*. Substrate *versus* velocity plots for the allosteric inhibition of TK-2 by the natural inhibitor Mg^{2+}-dTTP and T-α-CNP using the mixed model inhibition of GraphPad (Fig. 3; Table S5). Panel *D*. 2'-Deoxycytidylate deaminase (dCMPD) activity at varing dCMP substrates in the presence of a fixed concentration (250 µM) of the natural allosteric inhibitor dCTP. K_m for dCMP was calculated to be ~120 µM. Panel *E*. Inhibitory effect of the L-enantiomeric C-α-CNP on the allosteric stimulation of

dCMPD by dCTP. Varying concentrations of C-α-CNP were exposed to the enzyme for 10 min in the presence of different dCMP concentrations (25 to 100 μM) in the presence of one fixed Mg^{2+}-dCTP (250 μM) concentration. The stimulatory effect of dCTP on dCMPD was dose-dependently inhibited by C-α-CNP. Data are the mean ± SD of at least 2 to 3 independent experiments.

Table S1. Inhibitory activity of the L-enantiomeric α-CNPs against HIV-1 RT in the presence of different homopolymeric template/primers

Compound[a]	IC_{50}[b] HIV-1 reverse transcriptase (μM)		
	poly rA.dT ([^{3}H]dTTP)	poly rI.dC ([^{3}H]dCTP)	poly rU.dA ([^{3}H]dATP)
T-α-CNP	**0.41 ± 0.08**	>500	155 ± 147
U-α-CNP	**3.0 ±1.6**	>500	208 ± 72
C-α-CNP	164 ± 22	**4.3 ± 0.3**	45 ± 0
A-α-CNP	>500	>500	**0.19 ± 0.11**
AZT-TP	0.11 ± 0.05	-	-
ddCTP	-	14 ± 1	-
ddATP	-	-	1.5 ± 0.24

[a]Each α-CNP represents as a pair of diastereomers at the alpha-carboxy stereocenter.

[b]50% Inhibitory concentration, or compound concentration required to inhibit polymerase activity by 50%. Data are the mean ± SD of at least 2 to 4 independent experiments.

Inhibition of RTs by T-, U-, C-, and A-α-CNP analogues was evaluated using the respective homopolymeric template/primers poly rA.dT (for T- and U-α-CNP), poly rI.dC (for C-α-CNP), and poly rU.dA (for A-α-CNP) and ~1.25-2.5 μM of their appropriate corresponding dNTP substrates [CH_3-^{3}H]dTTP (for T- and U-α-CNP), [5-^{3}H]dCTP (for C-α-CNP), and [2,8-^{3}H]dATP (for A-α-CNP).

Table S2. Kinetic parameters for T-α-CNP, AZT-TP and INDOPY-1 inhibition of HIV-1 RT as derived from non-linear regression analysis (GraphPad Prism 5).

	Mode of inhibition	**K_i[a] (μM)**	**K_m[b] (μM)**	**Alpha-value[c]**	**R^2-value[d]**
T-α-CNP / dTTP[e]	Competitive	0.283 ± 0.050	6.03 ± 1.31	3.29	0.964
T-α-CNP / Poly rA.oligo dT[f]	Uncompetitive	0.330 ± 0.022	0.868 ± 0.089	0.691	0.983
AZT-TP / dTTP[e]	Competitive	0.015 ± 0.002	4.29 ± 0.34	~1.27×10^{22}	0.982
AZT-TP / Poly rA.oligo dT[f]	Non-competitive	0.003 ± 0.0003	0.688 ± 0.121	1.07	0.977
INDOPY-1 / dTTP[e]	Competitive	0.168 ± 0.025	2.10 ± 0.31	87.9	0.980
INDOPY-1 / Poly rA.oligo dT[f]	Uncompetitive	0.908 ± 0.043	1.87 ± 0.13	0.150	0.997

[a] K_i, inhibition constant.

[b] K_m, Michaelis-Menten constant.

[c] Alpha-value determines the most likely kinetic mechanism.

[d] R^2-value represents a parameter for the goodness of curve fit.

[e] Varying dTTP and drug.

[f] Varying Poly rA.oligo dT and drug.

Table S3. X-ray data and refinement statistics for the HIV-1 RT/ds DNA/T-α-CNP complex

	HIV-1 RT/dsDNA/T-α-CNP
PDB ID	4R5P
Data collection	
Space group; Cell dimensions	$P2_1$
a, *b*, *c* (Å)	89.9, 134.0, 139.2
α, β, γ (°)	90, 97.81, 90
Resolution range (Highest resolution shell) in Å	50 – 2.9 (2.95 – 2.90)
R_{merge}	0.107 (0.634)
$I / \sigma(I)$	8.9 (1.9)
Completeness (%)	99.6 (99.2)
Redundancy	4.0 (3.4)
Refinement	
Resolution (Å)	44 – 2.9
Cut-off criteria	F ≤ 0
No. reflections (R_{free} set)	72,084 (2,151)
R_{work} / R_{free}	0.199 (0.251)
No. atoms refined	17,726
Stereochemistry (RMSDs)	
Bond lengths (Å)	0.01
Bond angles (°)	1.51

Table S4. Inhibitory activity of thymine, cytosine and adenine α-CNPs against mutant HIV-1 reverse transcriptases

HIV-1 RT	Fold decreased activity compared to wild-type RT[a]					
	Poly rA.dT + [^{3}H]dTTP		Poly rI.dC + [^{3}H]dCTP		Poly rU.dA + [^{3}H]dATP	
	T-α-CNP	INDOPY-1	C-α-CNP	INDOPY-1	A-α-CNP	INDOPY-1
M184V	16	7.1	11	>6.7	1.7	NA[b]
Y115F	2.4	2.8	1.1	2.9	0.79	NA

[a]Ratio of IC_{50} mutant RT/IC_{50} wild-type RT. Values were derived from the mean of at least 3 independent experiments.

[b]Not active.

Table S5. Kinetic parameters for dTTP and T-α-CNP inhibition of TK-2 as derived from non-linear regression analysis (GraphPad Prism 5)

	Mode of inhibition	**K_i[a] (μM)**	**K_m[b] (μM)**	**Alpha-value[c]**	**R^2-value[d]**
dTTP / dThd[e]	Competitive	0.927 ± 0.068	1.33 ± 0.126	~ 3.15×10^{16}	0.991
T-α-CNP / dThd[f]	Non-competitive	125 ± 9.9	2.64 ± 0.27	1.24	0.977

[a] K_i, inhibition constant.

[b] K_m, Michaelis-Menten constant.

[c] Alpha-value determines the most likely kinetic mechanism.

[d] R^2-value represents a parameter for the goodness of curve fit.

[e] Varying the substrate dThd and dTTP.

[f] Varying the substrate dThd and T-α-CNP.

Table S6. Comparative overview of the properties of α-CNP and other HIV RT inhibitor classes

	α-CNP[a]	NRTI/NtRTI[b]	NNRTI[c]	NcRTI[d] (INDOPY-1)
Nucleos(t)ide structure	Yes	Yes	No	No
Metabolic conversion required	No	Yes	No	No
Enzyme inhibition *versus* dNTP substrate	Competitive	Competitive	Non-competitive	Competitive
Binding to RT substrate-binding site	Yes	Yes	No	Yes
Nature of the RT binding	Mutually exclusive with dNTP, but coordinating with Mg^{2+}	Mutually exclusive with dNTP, but coordinating with Mg^{2+}	Mutually exclusive with dNTP and Mg^{2+}	Mutually exclusive with dNTP and with Mg^{2+}
Nucleobase-specific binding to template	Yes	Yes	No	No (but better after T or C than after G or A)
Binding location	Post-translocation (N) site[e]	N site	NNRTI-binding site	N site
DNA chain termination	No	Yes	No	No
Selective for HIV-1 RT	No	No	Yes (HIV-1)	No

[a]α-Carboxy nucleoside phosphonate.

[b]Nucleos(t)ide RT inhibitor (e.g. zidovudine triphosphate or tenofovir diphosphate).

[c]Non-nucleoside RT inhibitor (e.g. nevirapine or rilpivirine).

[d]Nucleoside competitive RT inhibitor (e.g. INDOPY-1).

[e]T-α-CNP binds the RT/nucleic acid complex in its post-translocated conformation, analogous to the binding of a dNTP. In contrast, foscarnet (a pyrophosphate analogue) has shown to trap the pre-translocated RT/nucleic acid complex (1).

1. Marchand B, Tchesnokov EP, Götte M (2007) The pyrophosphate analogue foscarnet traps the pre-translocational state of HIV-1 reverse transcriptase in a Brownian ratchet model of polymerase translocation. *J Biol Chem* 282:3337-3346.